noted
Draft Copy

2/3/8 ① AB 2182

MECHANICS OF BRITTLE MATERIALS

PART I. PRELIMINARY MECHANICAL
PROPERTIES AND STATISTICAL REPRESENTATIONS

OCTOBER 1973

ARMY MATERIALS & MECHANICS RESEARCH CENTER

WATERTOWN, MASSACHUSETTS   02172

DTIC
SELECTE
S APR 1 1982 D
A

ARPA Order Number 2181
Program Element Code: 61101D
Project Code Number 2D10
Agency Accession Number DA OD 4733

82 03 30 086

TABLE OF CONTENTS

82 03 30 086

LIST OF ILLUSTRATIONS

LIST OF TABLES

1.0 INTRODUCTION

The necessity to cope with temperatures beyond the capabilities of most metallic materials is the impetus to use the so-called brittle ceramics. Typical of such applications are re-entry vehicles (leading edge elements, nose caps, control surface panels, etc.) and propulsion systems (rocket engine nozzles, combustion chambers, etc.). Most recently, however, application of ceramics to high temperature gas turbine engines has provided additional stimulus to further develop design and analysis methodology for brittle materials.

For example, Ford Motor Company and Westinghouse Electric Corporation have had research programs underway for several years on the application of ceramics to turbine engines. In June of 1971, the Advanced Research Projects Agency of the Department of Defense sponsored a contract to accelerate this work, and to demonstrate that brittle materials can be successfully utilized in demanding high temperature structural applications. Two demonstration items were chosen, namely a vehicular gas turbine and portions of a large turbine power generator with emphasis on the former.

Thus far a number of contractor reports have been published on the ARPA-FORD-WESTINGHOUSE project(1)*. In addition, many hundreds of hours have been accumulated in hot engine test rigs on various first and second stage stators and rotors, shrouds, nose cones, and combustion chambers, regenerator seals, etc. The engine project is strongly oriented toward an experimental-trial assessment of iterative designs. This also allows proof testing of individual components, prior to assembly for a required

---

* Numbers in parenthesis pertain to references

1

200 hour engine operation demonstration test.

In addition to duties as contract monitors on this project, the Army Materials & Mechanics Research has been conducting in-house research in support of the project. This report documents portions of the AMMRC studies completed during the period May 1972 to May 1973. The overall research consists of theoretical and experimental investigation of constitutive equations, fracture mechanics, failure theories, thermal and mechanical fatigue and probabilistic aspects of brittle material behavior. Materials to be investigated include several types of silicon nitride and silicon carbide. Under ARPA sponsorship the Ford-Westinghouse team is conducting an extensive program of mechanical and physical properties determination for the candidate ceramic materials. However much additional information ought to be developed and considerable effort is required to further refine design and analysis procedures for such materials.

2.0 MECHANICAL PROPERTIES CHARACTERIZATION

During this project a number of test methods are being employed to study response of the ceramic materials. Behavior under simple monotonic loads is being observed via two types of tension tests (including hydroburst of thin walled rings) and several types of flexure loadings and specimen sizes. Results obtained to date have been at ambient laboratory conditions (73°F).

Tension experiments were completed on specimens of the type shown in Figure 1. These dogbone configurations are subjected to hydrostatic pressure in the apparatus shown in Figure 2. The ratio of shoulder to gage section diameter is selected to minimize the amount of pressure required to fracture the specimens in tension. Furthermore the specimen ends ride on "0"-ring seals and bending effects therefore tend to be reduced by this test method.

2.1 TENSION TESTS ON HOT PRESSED SILICON NITRIDE (NORTON HS-130)

Sixteen specimens of the design and method given in AMMRC-TR 69-02 and shown in Figure 1 were tested to failure. The first specimen tested was in the as-received condition such that circumferential (perpendicular to the load axis) score (grinding marks existed all along the gage length. (See Figure 3). Accordingly the specimen failed at 38,160 psi. The next specimen to be tested was first carefully hand-polished using diamond grit and it failed at 54,700 psi. Subsequently a simple polishing machine was constructed to prepare the remaining specimens. The resulting data is tabulated next.

TABLE 1 TENSION TEST RESULTS HOT PRESSED SILICON NIRIDE

Specimen	Initial Dimensions Diameter	Eccentricity	After Polishing	Strength psi	Remarks
2	.2000	.0003	.1990		
3 a)	.1998	.0001	.1995	65,460	b) broke inside gage section (g.s.)
4 a)	.2000	.0003	.1990	85,410	c) broke at shoulder tangent (S.T.)
5 a)	.2008	.0006	.1990	73,540	b) broke inside g.s.
7	.1995	.0005	.1990	46,060	c) broke in 3 parts in shoulder fillet (s.f.)
9 a)	.1998	.0002	.198-.1975	69,820	b) broke in g.s.
10 a)	.1995	.0002	.1990	76,770	c) broke in g.s.
11 a)	.2003	.0001	.2000(hand lap)	54,700	c) broke in g.s.
12 a)	.2003	.0006	.1985 - .1980	65,390	c) broke in s.f. at scratch
14 a)	.2000	.0011	.1990	63,030	c) broke in g.s.
15	.1990	.0003			
16 a)	.2000	.0007	.1980	52,670	c) broke at s.t.
17 a)	.2003	.0005	.1980-.1975	78,400	c) broke in g.s.
18	.2000	0			
19	.2000	.0001	Machine Finish	38,160	c) broke in 3 parts in S.f.
20 a)	.1998	.0002	.1975	63,620	c) broke in s.f.
21 a)	.2010	0	.198	62,880	b) broke in g.s.
22 a)	.2005	.0001	.1990	61,820	c) broke in 3 parts s.t.

Notes; a) Values used in Weibull statistics; b) internal fracture origin; c) surface fracture origin

ENLARGED VIEW
OF
ELLIPTICAL FILLET

45°

.7373 — TO TANGENT POINTS

Y

X

$\frac{1}{16}$ R

32

.200-.001

GAGE
SECTION

$1\frac{1}{2}$ REF

$\frac{1}{16}$

$\frac{5}{8}$

THIS DISTANCE
$4\frac{3}{4}$

$\frac{5}{8}$

ELLIPTICAL FILLET
MAJOR AXIS — 1.5
MINOR AXIS — .28

.996-.001
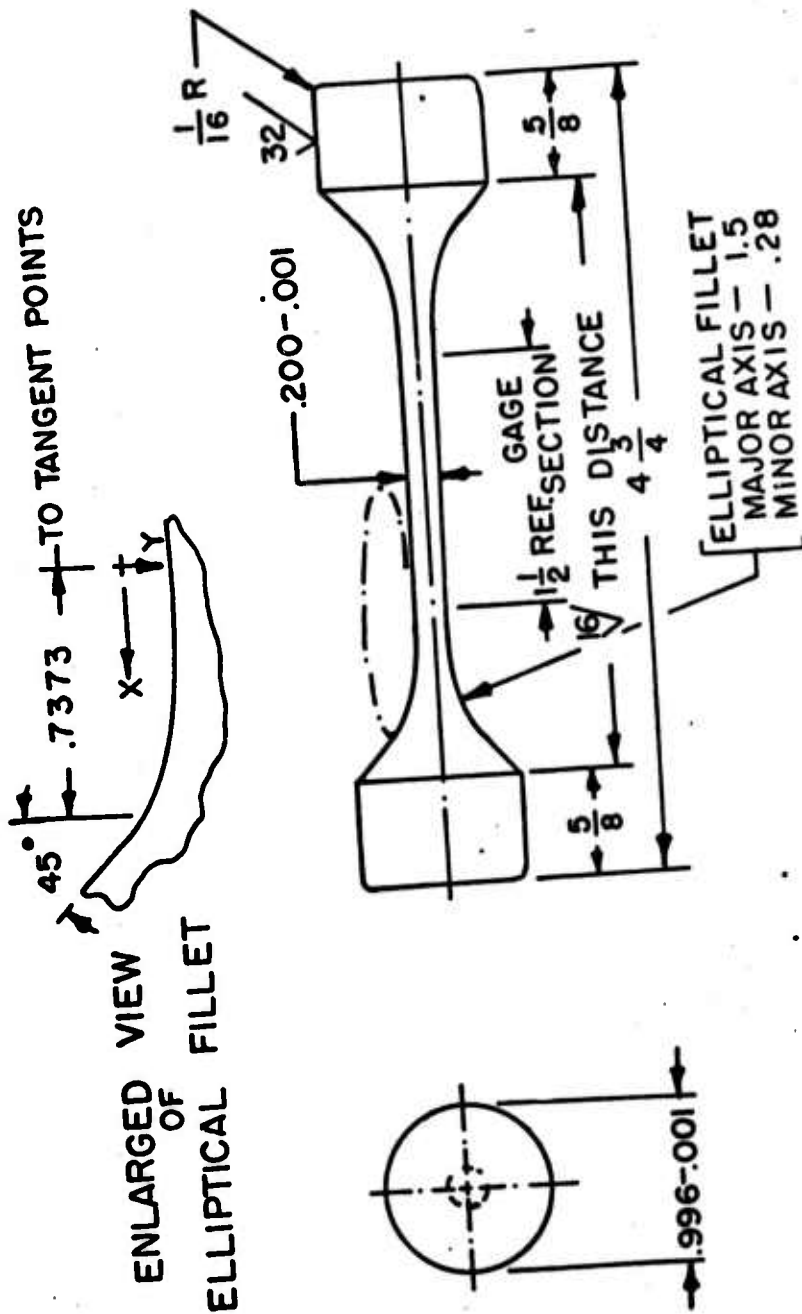
NOTE :-
NO MISMATCH ALLOWED AT TANGENT POINTS
DIAMETERS TO BE CONCENTRIC WITHIN .0005 TIR
MAXIMUM TOOL RADIUS :- .062
CENTERS PERMISSABLE
REDUCE DIAMETER .001 AT MIDDLE OF GAGE SECTION LENGTH. TRANSITION
TO BE GRADUAL TO AVOID DISCONTINUITIES

Figure 1.

5
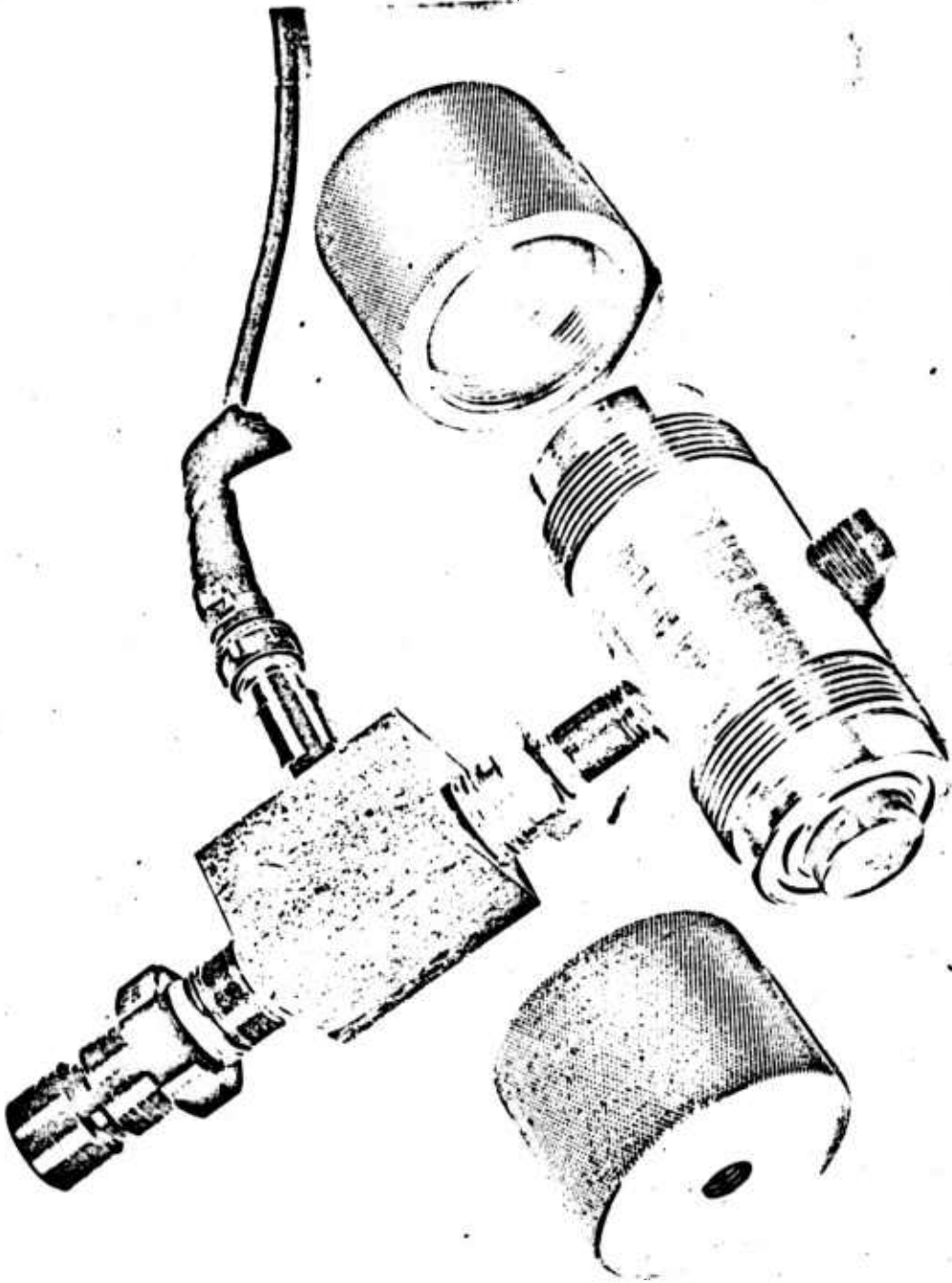
IMPROVED TEST SYSTEM - TENSION TEST FOR BRITTLE MATERIALS. END CAPS REMOVED TO SHOW SPECIMEN IN TEST POSITION

Figure 2
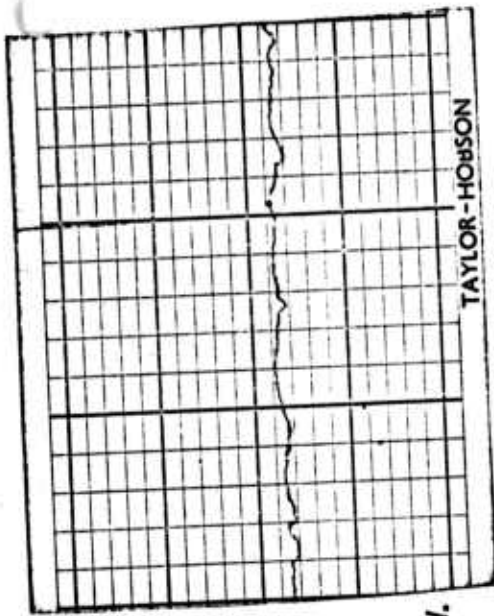
50X 10^{-6}inch/div.

.0125"/div.
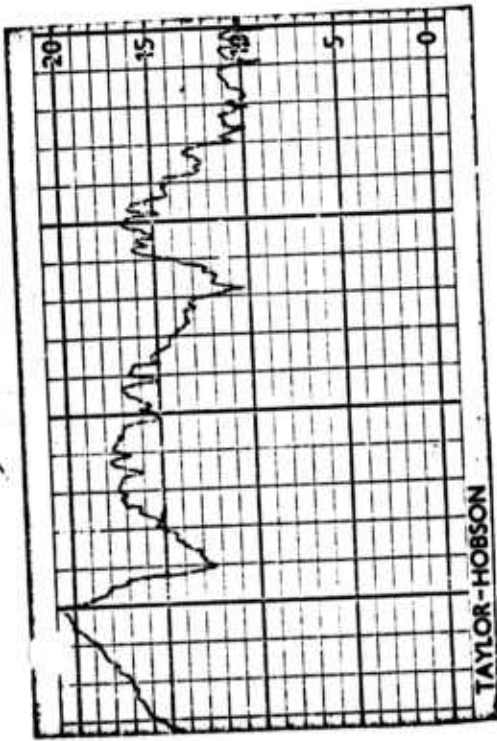
Tally-Surf Measurements
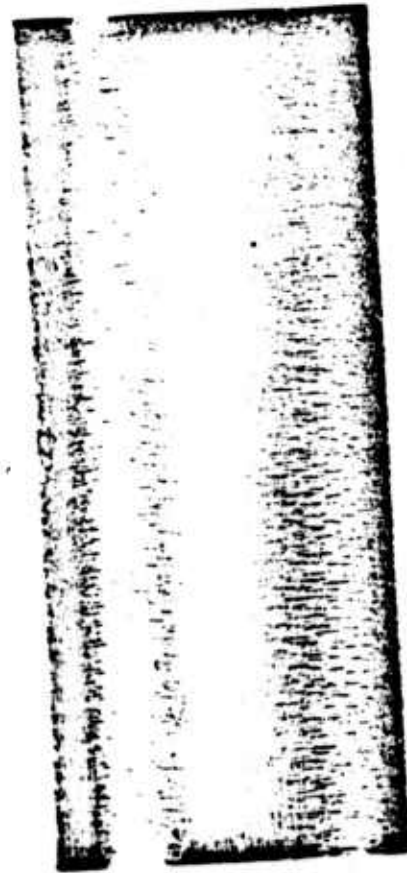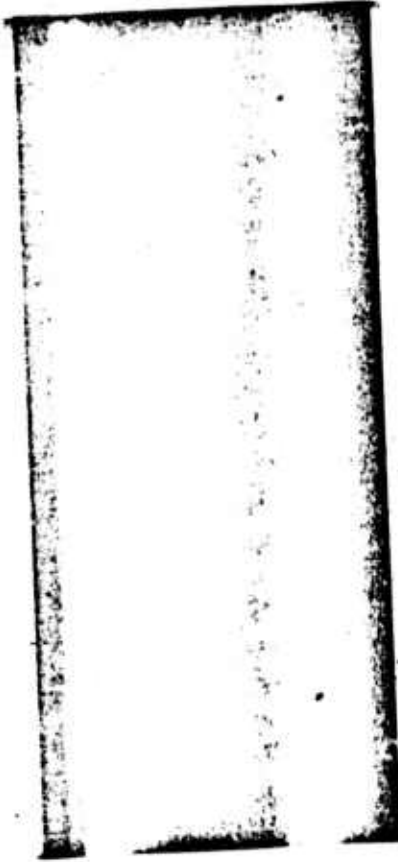
SILICON NITRIDE SPECIMEN 10 X
surface finish produced by lapping

SILICON NITRIDE SPECIMEN
surface finish produced by grinding

Figure 3. Photomicrograph of Typical Tension Specimen Surface, As-ground and Polished.

7

Another attempt was made to improve over the as-received surface integrity by use of chemical vapor deposited (CVD) Silicon Nitride coatings on the HPSN. Two tension specimens were coated at United Aircraft Research Laboratories. Hopefully the CVD coating would provide an inexpensive method of improving the surface integrity of the HPSN, rather than costly polishing procedures. Unfortunatley one of the specimens was destroyed during the CVD process. The other was returned intact, however the shoulder region was eroded. Subsequently this specimen failed at 33,600 psi. Inspection of the fracture surface revealed a fairly uniform deposit of silicon nitride having a nominal thickness of 4 mils. There was an obvious interface of diss milar material and fracture had been initiated at a flaw of nominal size .013 X .075 inches, located just beneath the coating in the mid-portion of the gage section. Obviously further development of the CVD process is required to achieve a successful compatible coating procedure.

2.2 FLEXURE OF HOT PRESSED SILICON NITRIDE (Norton HS-130)

Beam bending experiments were conducted on HPSN using 1/4 point loading on rectangular specimens each 3 1/4" X 0.15 X 0.60 inches. The beams were carefully ground by Norton Company and no extra surface polishing was attempted. The test apparatus is illustrated in Figure 4. and the resulting data is tabulated next. Specimens were instrumented with strain gage rosettes both top and bottom of the beam in order to measure poisson's ratio and to compare the tension and compression modulus.
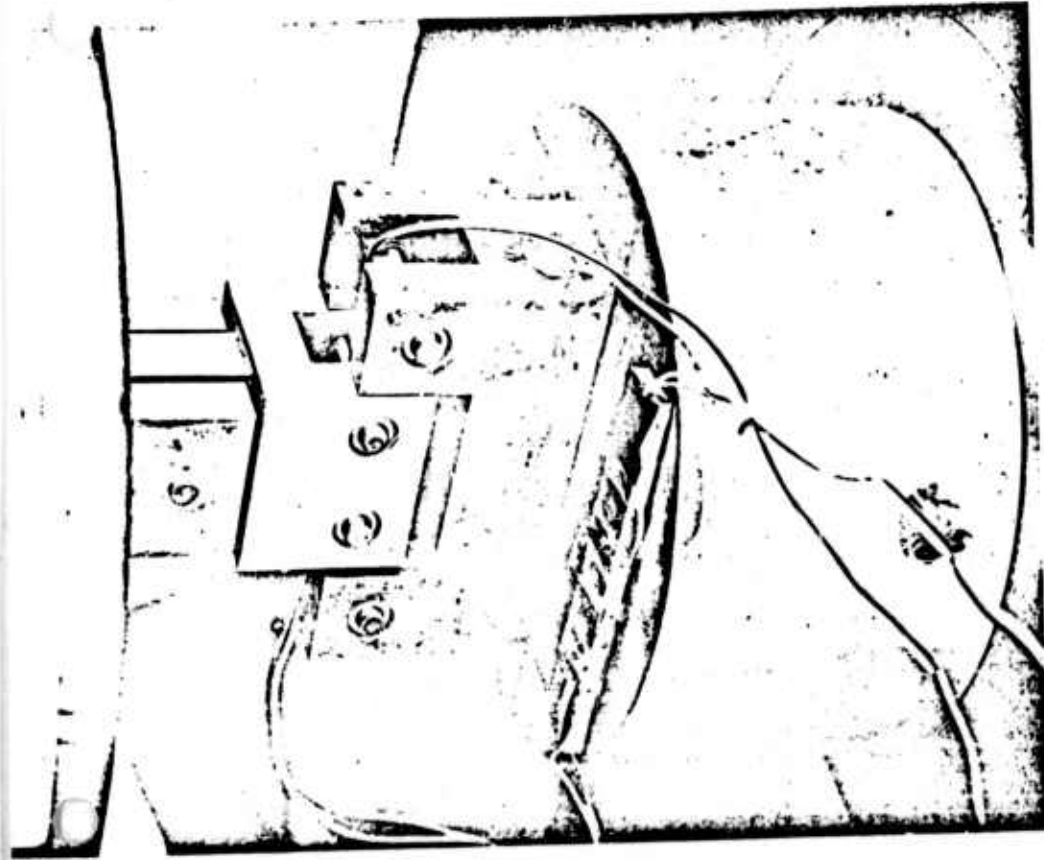
PINS RESTING
ON
ROLLER BEARINGS
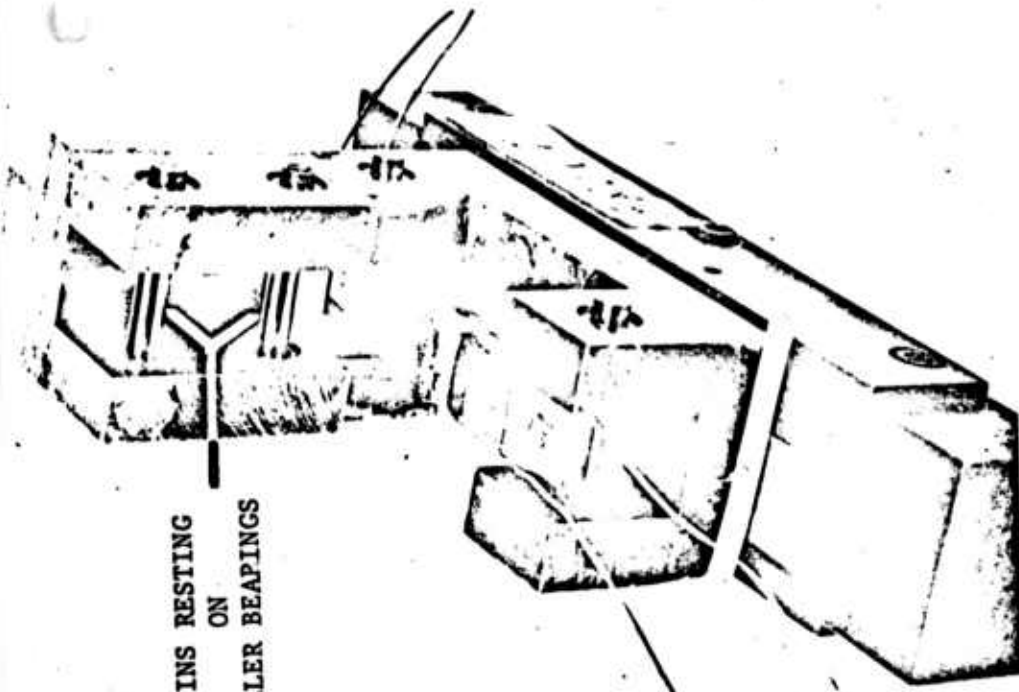
"FRICTION FREE" FIXTURE.

BEND TEST SETUP.

BEND TEST SETUP EMPLOYING "FRICTION FREE" FIXTURE SHOWING
SPECIMEN UNDER LOAD. DOUBLE POINT LOADING. 0.150 x 0.600
x 3-1/4-INCH SPECIMEN.

Figure 4. Flexure Fixture.

9

TABLE 2 SUMMARY OF FLEXURE TESTS HPSN
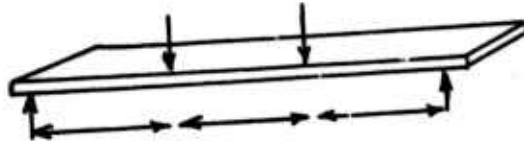
Specimen	Modulus X10⁻⁶ psi	Strength ksi	Remarks
1*	44.44	88,889	Broke out of g.s.
2*	44.44	88,889	"
3	46.78	98,889	
4	46.18	97,222	Badly chipped beam edges
5	45.38	74,167	Broke under roller
6*	45.40	64,440	
7	46.47	95,277	Chipped edges
8	45.40	82,778	
9	46.54	109,444	
10	46.00	95,556	
11	45.94	100,000	
12	47.03	95,833	Badly chipped edges
13	45.82	72,222	
14	46.3	85,111	
15	47.03	100,722	
16	46.36	106,667	
17	46.36	101,389	
18	46.54	107,611	
19	45.82	103,194	
20	44.89	96,444	
mean*	46.167	95,443	
standard deviation	.568	10,542	
variance %	1.23%	11.045%	

*Not including

ROUND BEAM TESTS

A number of the hot pressed silicon nitride tension specimens fractured leaving fairly large portions of the straight-sided gage section intact, and it was decided to perform flexure experiments on these fragments. Four point bend tests were performed on eight specimens using the loading span indicated in the sketch.
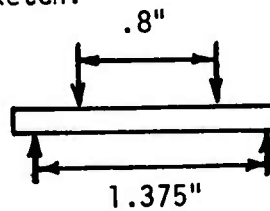
TABLE 3

The experiments used rigidly fixed upper and lower loading heads and were completed in a 20,000 lb. capacity Instron using a 1000 pound load cell.

Specimen	Diameter	Failure Load (lb)	Strength	Remarks
19	.200	323	59,120	As machined finish
20	.1975	518	98,460	
9	.198	722	136,190	Results questionable, bad cell unbalanced
4	.1995	450	82,980	
12	.1985	450	84,240	Break near load point
16	.200	358	65,520	" " " "
22	.198	422	79,600	
7	.199	450	83,610	

For specimens 20, 4, 22 and 7
mean = 86,163
standard deviation = 7262
coefficient of variation = 3.43%

For all specimens except #19
mean = 82,401 psi
standard deviation = 9625
coefficient of variation = 11.68%

2.3 Reaction Bonded Silicon Nitride (RBSN) (Ford Material)

A series of molds were obtained from Reliable tool & Die Company*
for injection molding of five types of RBSN specimens using the Ford
Motor Company proprietory process. The molds were supplied to Ford
and beams, rings, tension dog bones (See Figure 1) and compact tension
plates were prepared. The ring specimens were unsuccessful due to
cracking associated with shrinkage, the tension dogbones partially
successful and the beams and plates appeared adequate. It should be
noted that the processing of this material is improving as time proceeds
and therefore the results reported herein are representative of a first
generation material. At a later date additional specimens will be
prepared using improved production techniques.

*Reliable Tool & Die Company, Dearborn, Michigan

Tension Tests

The RBSN specimen dimensions prior to testing are as indicated below:
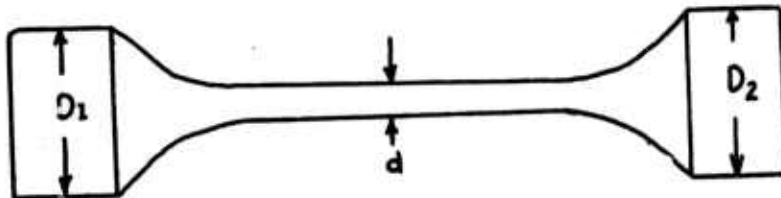
TABLE 4

#	D1	D2	d	(Eccentricity run-out)	Tensile Strength, psi
1	.995	.9955	.2 to .188	*	7460
2	.996	.995	.184 to .195	.003	7460

As stated these specimens were injection molded. It appears that when cast there was a mismatch in the die which caused the diameters to be egg shaped. Also run out between diameters "D_1" and "d" was considerable. To correct some of the run out, diameters "D_1" were turned down to a smaller size, built up with epoxy, and remachined in relation to diameter "d". Because of considerable mismatch in specimen #1, diameter "d" still appeared egg shaped and it was impossible to obtain a true run out reading.

Due to noncircularity as well as eccentricity, poor strengths were achieved. Examination of the fracture surfaces showed gross defects as depicted schematically in Figure 5.
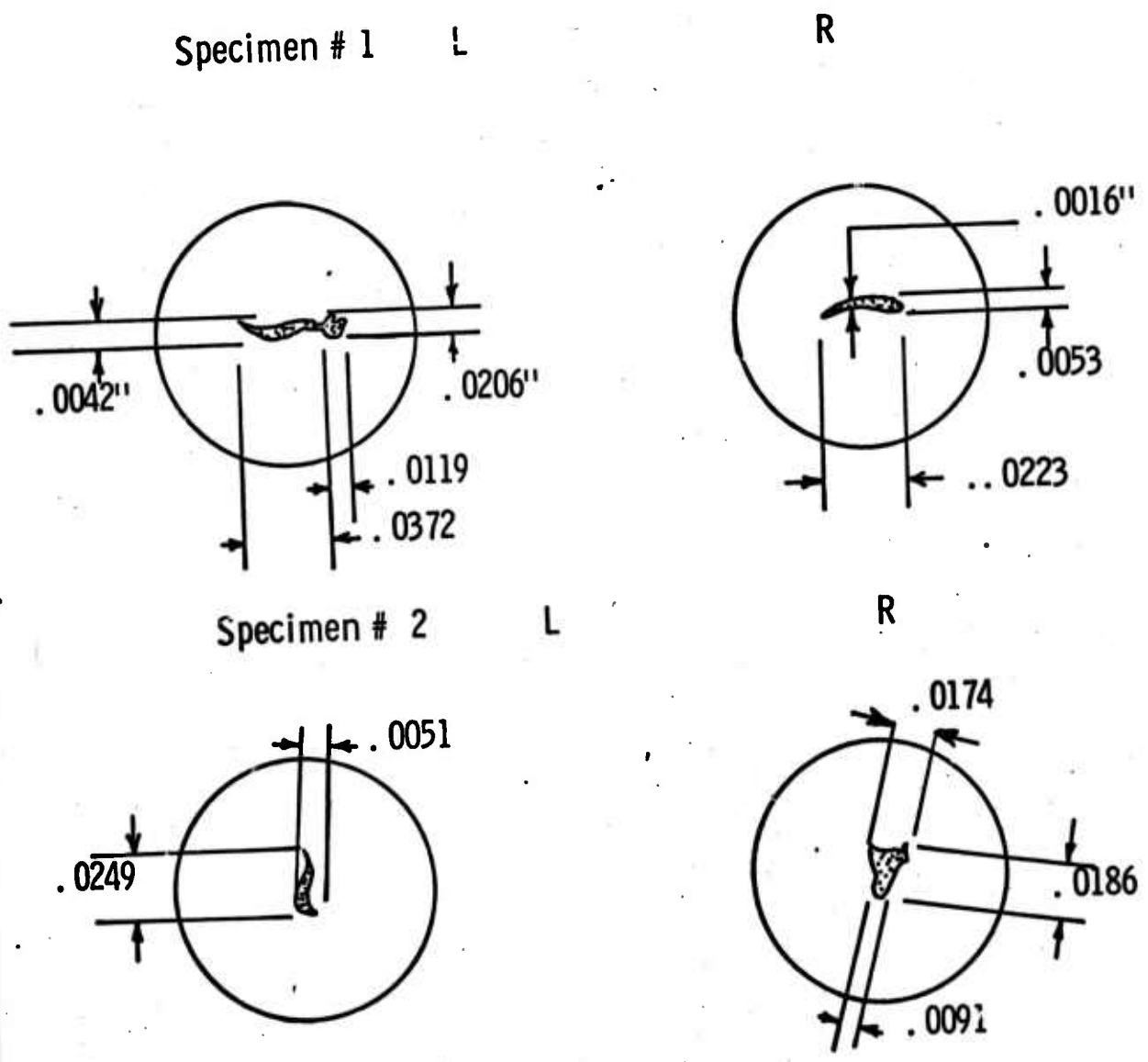
Specimen # 1   L   R

Figure 5. Schematic of Flaws in Reaction Bonded Silicon   Nitride
Tension   Specimens.

14

2.4 Flexure Tests on Reaction Bonded Silicon Nitride (RBSN) (Ford Material)

Flexure tests were also completed at room temperature on RBSN using the injection molded and nitrided specimens supplied by Ford. Both rectangular and approximately circular specimens were used. The data is listed next.

FLEXURE ON REACTION SINTERED SILICON NITRIDE

3.25 X .15 X .6 inch Beams   1/3 point loading

1.0"   1.0"   1.0"
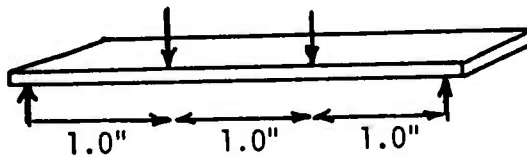
TABLE 5

Specimen	Modulus X 10^{-6} psi	Strength, psi
1	13.96	15,556
2	13.58	12,444
3	13.80	14,667
4	14.78	16,000
5	13.89	13,556
6	15.65	16,111
7	15.15	15,333
8	14.34	16,889
9	13.58	14,778
10	14.54	15,611
11	15.40	14,778
12	14.58	15,111
13	14.29	16,556
14	12.84	11,444
15	14.19	
16	14.67	
17	14.19	

mean = 14,917 psi

standard deviation = 1,474

variance = $\frac{1,474}{14,917}$ = .098813 = 9.9%

14.32 X 10^6 = mean

.6851 = standard deviation

4.78% variance

ROUND BEAMS
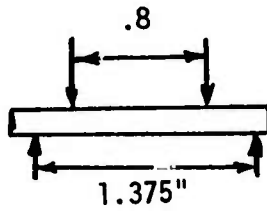
Three round beam specimens were also subjected to flexure tests. These specimens were obtained from tension specimens which were broken unintentionally prior to tensile testing. The flexure loading just described was also used.

TABLE 6

Specimen	Dia	Failure Load (lb)	Strength
1	.195	78	15,400
2	.195	74	14,610
3	.195	85	16,790

All breaks occured in the constant moment section.

2.5 NONDESTRUCTIVE EVALUATION

The original material billets as well as final machined specimens have been nondestructively examined. Ten billets of hot pressed Norton HS130 silicon nitride, each six inches square and nominally one and an eighth inch thick were subjected to x-ray radiography as well as ultrasonic characterization. A number of the billets are in the process of being machined into beams, tension and torsion specimens, compact tension specimens (Figure 6) and notched beam "work of rupture" specimens. The available specimens have been destructively tested as reported. In general both the X-ray and ultrasonic inspection revealed uniform quality material. Some small regions of high density were observed by X-rays.

Ultrasonic compressional wave veloicty measurements were made in the plane and perpendicular to the plane of the compact tension crack growth specimens (See Figure 6). The average velocities suggest a slightly higher modulus might exist along the pressing direction.

2.5.1 HYDROBURST SPECIMENS

In addition to the attempt to produce RBSN rings, three other materials were considered, namely HPSN, chemical vapor deposited silicon carbide and silicon nitride.

Thirty of the hot pressed silicon nitride rings were obtained from Norton Co. and subjected to X-ray radiography, local ultrasonic compression and shear wave measurements and "C"-scan observation. The X-ray examination served to locate several high density regions. The "C"-scan results appear in Figures 7 and 8. These two illustrations illustrations represent "C"-scan observations where the rings were merely reversed in the test apparatus.

17

4. 25"

.375" dia.

4. 14 x 10⁵ in. /sec.

3. 7X 10⁵ in. /sec.

2. 25"

3. 85X 10⁵ in. /sec.
Ultrasonic compression wave
velocity.
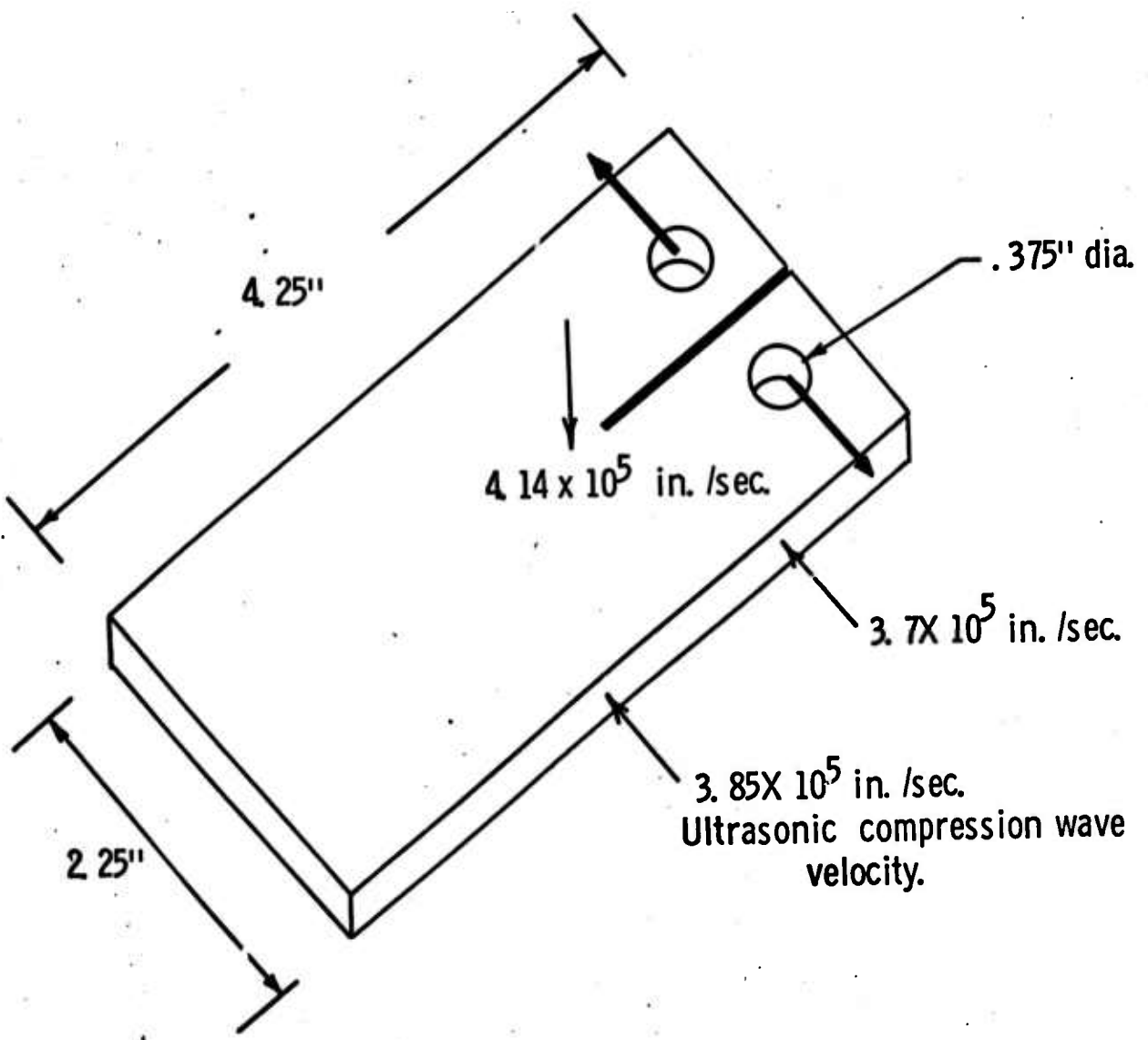
Figure 6. Compact Tension Crack :Propagation Specimen
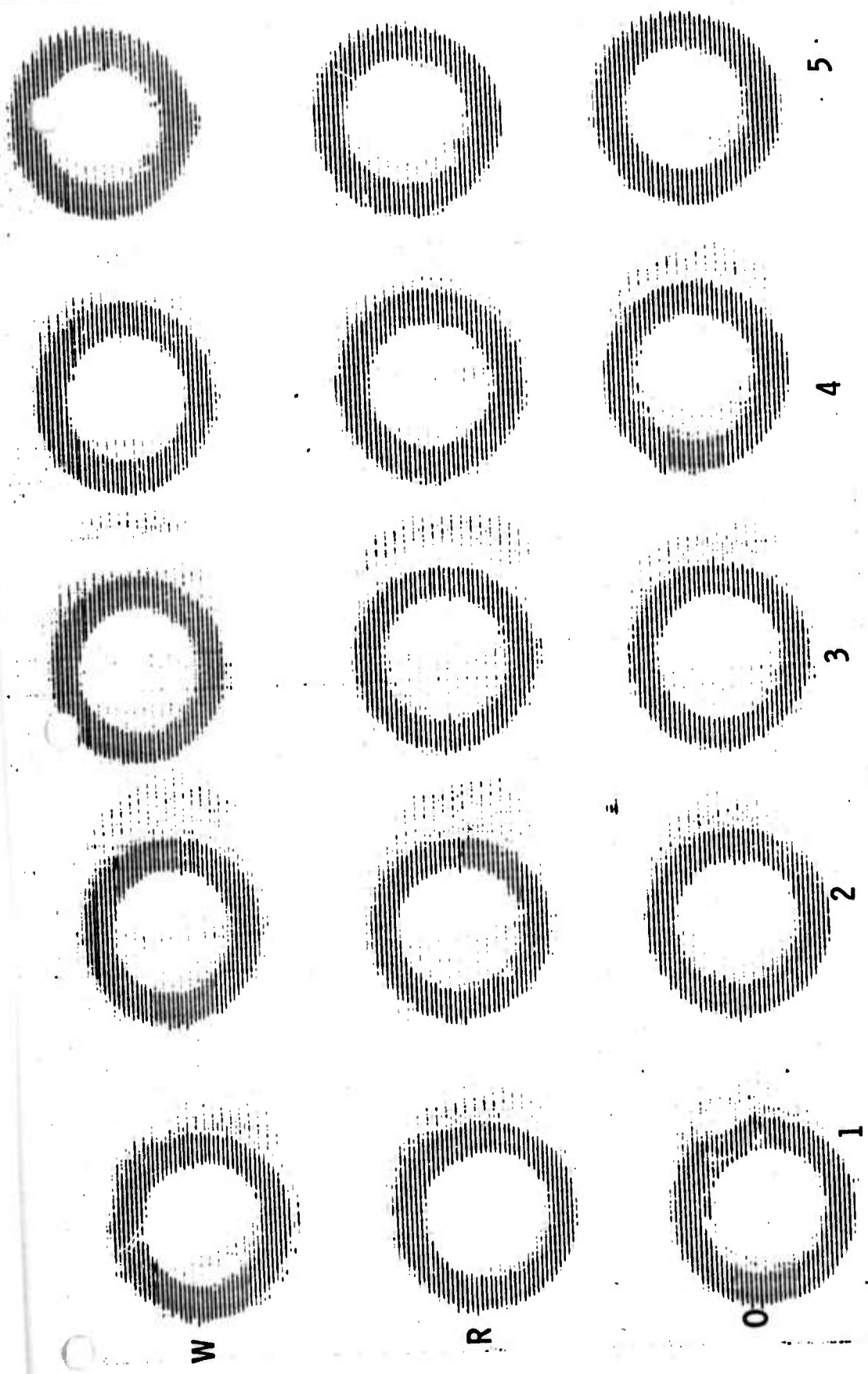
Figure 7. "C" Scan Observations, Hot Pressed Silicon Nitride Ring Specimens.
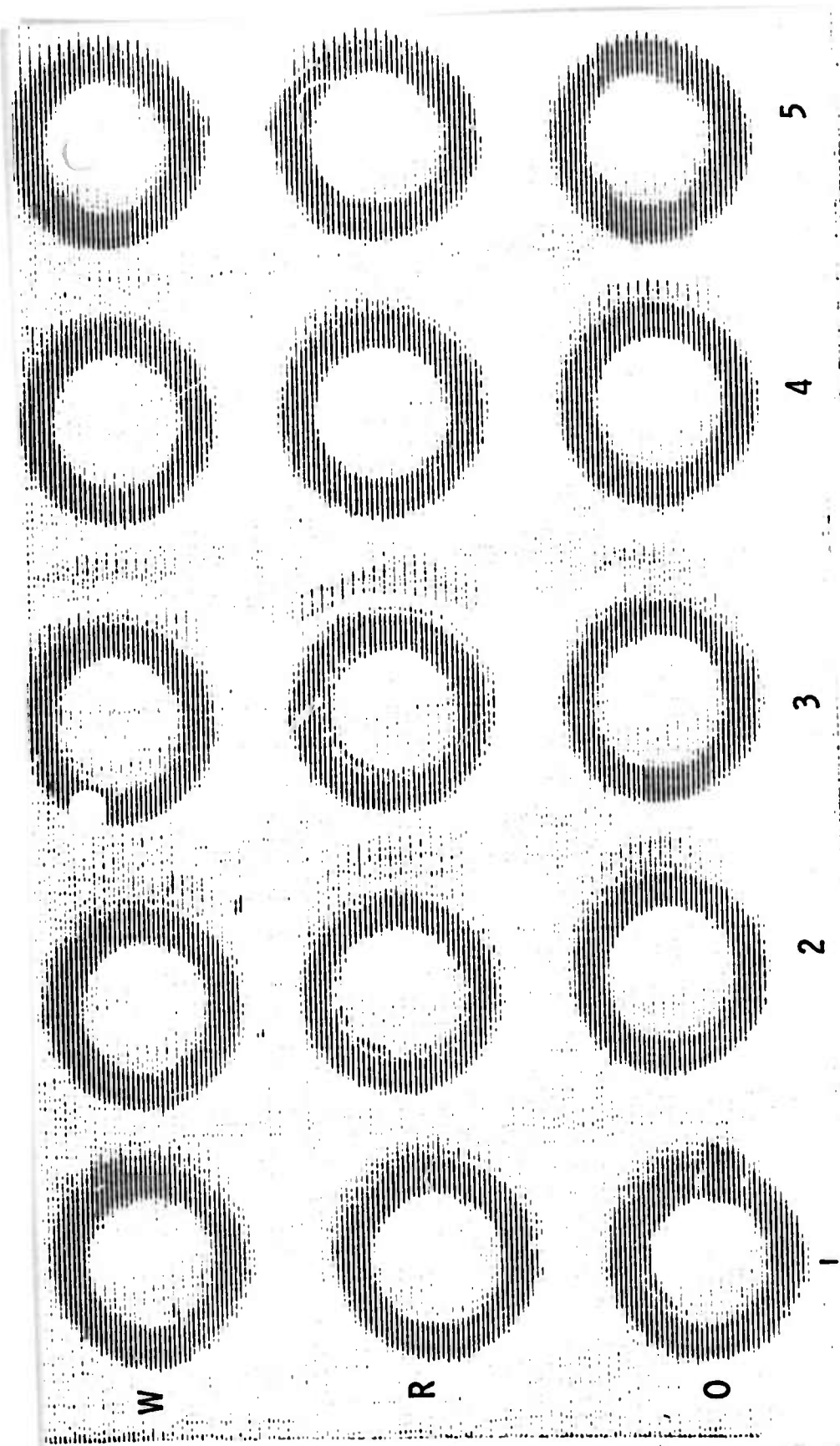
Figure 8 "C" Scan Observations, Ring Specimens, Reversed Orientation

20

The nondestructive evaluation of thirty rings yield the following defects in twelve rings

TABLE 7 SUMMARY OF DEFECTS IN RING SPECIMENS

Specimen	Nature of Defects
B-2	High density surface flaw on inside wall
Y-5	Two high density areas, approximately 180° apart
G1, 3 and 4	Outer wall high density surface flaws
W-4	High density surface flaw, inside wall
R-5	Several interior high density regions
0-2	Outer wall, high density flaw
0-3	Mid ring (interior) high density area
0-1	Worst "C" scan
Y-4	Bad "C" scan
G-4	Bad "C" scan
Y-5	Bad "C" scan, indications 180° apart

Note that "C" scanning appears to be sensitive to low porosity regions whereas X-ray radiography is suited to determine high density areas. These rings were prepared over sized (nominal dimensions 0.8" inside dia., 1.35" outside dia., x .625" high) in order that the specimens might be carefully machined to thin walled rings. During this machining process a number of the detected flaws will be removed. However the specimens which remain flawed will be subjected to detailed fractography in order to establish the significance of the various flaws.

Ultrasonic through transmission measurements were completed on a local, point-by-point basis using both compressional and shear waves. Each ring was tested through the wall thickness as well as through the height of the ring (which corresponds to the pressing direction of HPSN. The rings were systematically scanned and the high and low readings were recorded. Precise measurements of ring density were also completed. Using these observations and applying elementary formula of wave propagation theory, it was then possible to estimate young's modulus, shear modulus and poisson's ratio. The information is recorded in Table 8 and 9. At a later date the data will be correlated with destructive test results. At the present time the information can be used to estimate statistical variability of moduli in the Norton H5-130 material.

TABLE 8 ULTRASONIC WAVE MEASUREMENT THROUGH RING WALLS

HOT PRESSED Si_3N_4

SAMPLE		Longitude Time	Wall Thickness Inch	Density (gr/cm³)	Poisson's Ratio Average	Young's Modulus	Poisson's Ratio Aver. L-H	Young's Modulus
Y-1	H* L*	1.27616 1.24733	.276	3.1712	.2655	44.84 46.94	.2546	45.84
Y-2	H L	1.33864 1.29589	.28725	3.1707		44.14 47.10	.2719	43.53 46.45
Y-3	H L	1.33864 1.29588	.2875	3.1638		44.12 48.12	.2547	45.09
Y-4	H L	1.34459 1.30822	.2865	3.1614		43.39 45.84	.2644	43.49 45.94
Y-5.	H L	1.37313 1.24966	.2865	3.1731		41.76 50.42	.255	42.66 51.51
0-1	H L	1.39529 1.?4956	.28585	3.1725		40.25 50.19	.2807	38.90 48.51
0-?	H L	1.36063 1.31347	.2873	3.152		42.49 45.59	.2607	42.91 46.05
0-3	H L	1.28592 1.26716	.2752	3.1621		43.78 45.09	.258	44.46
0-4	H L	1.33487 1.28218	.28665	3.1695		44.19 47.89	.2657	44.17 47.87
0-5	H L	1.34191 1.27108	.287	3.1617		44.78 48.89	.2781	43.54 47.88
B-1	H L	1.26710 1.24649	.27425	3.1617		44.78 46.27	.2781	43.54 44.99
B-2	H L	1.26307 1.25002	.274	3.166		45.04 45.99	.2753	44.08 45.01
B-3	H L	1.34718 1.29102	.2745	3.1679		39.76 43.30	.2533	40.75 44.37
B-4	H L	1.26498 1.25362	.27425	3.1715		45.07 45.89	.2788	43.75 44.55
B-5	H L	1.35035 1.27945	.2875	3.1702		43.44 48.39	.2599	43.95 48.96

*NOTE: The rings were examined on a point-by-point basis and the high (H) and low (L) values were recorded.

23

R-1	H	1.36430	.286k5	3.1778	.2655	42.26	.2564	43.05
	L	1.26922				48.83		49.75
R-2	H	1.25542	.26915	3.1521		43.80	.2642	43.92
	L	1.22914·				45.69		45.82
R-3	H	1.23516	.269	3.1623		45.34	.2645	45.44
	L	1.22916				45.79		45.88
R-4	H	1.34405	.2875	3.1746		43.91	.2635	44.10
	L	1.30708				46.43		46.63
R-5	H	1.34402	.28595	3.1767		43.47	.256	44.32
	L	1.29289				46.98		47.89
W-1	H	1.36168	.28685	3.1778		42.63	.2538	43.65
	L	1.25821				49.93		51.13
W-2	H	1.33420	.2868	3.172		44.31	.2627	44.57
	L	1.29615				46.95		47.23
W-3	H	1.26367	.27415	3.193		45.43	.2746	44.54
	L	1.26127				45.61		44.71
W-4	H	1.34221	.2869	3.1786		43.91	.2755	42.95
	L	1.29485				47.18		46.15
W-5	H	1.37400	.2862	3.1799		41.71	.259	42.27
	L	1.28058				48.02		48.66
G-1	H	1.35075	.287	3.1725		43.30	.2594	43.85
	L	1.28892				47.55		48.15
G-2	H	1.36075	.286	3.1776		42.44	.2788	41.20
	L	1.27263				48.52		47.10
G-3	H	1.36900	.28635	3.1606		41.80	.2735	41.08
	L	1.28137				47.72		46.89
G-4	H	1.37902	.28675	3.1824		41.60	.2801	40.26
	L	1.26557				49.39		47.80
G-5.	H	1.26017	.2732	3.1566		44.85	.258	45.55
	L	1.25224				45.42		46.13

TABLE 9 ULTRASONIC WAVE MEASUREMENTS THROUGH RING HEIGHT

HOT PRESSED Si_3N_4 RINGS

SAMPLE		Longitude Time	Shear Time	Thickness Inches	Density (gr/cm^3)	Young's Modulus	Longitude Velocity	Shear Velocity	Poisson's Ratio
Y-1	H	2.65710	4.62573	0.5798	3.1712	46.74	436416	250685	.2538
	L	2.65113				46.80	437398	250685	.2554
Y-2	H	2.64583	4,72440	0.5794	3.1707	45.37	437972	245280	.2715
	L	2.64274				45.40	438484	245280	.2723
Y-3	H	2.66029	4.63189	0.5797	3.1638	46.49	435817	250308	.2539
	L	2.65469				46.55	436736	250308	.2554
Y-4	H	2.69118	4.72475	0.5799	3.1614	44.90	430963	245473	.2599
	L	2.65673				45.21	436552	245473	.2688
Y-5	H	2.66045	4.63124	0.5800	3.1731	46.69	436016	250473	.2537
	L	2.65098				46.78	437574	250473	.2563
0-1	H	2.64314	4.77664	0.5798	3.1725	44.75	438721	242765	.2793
	L	2.63200				44.84	440578	242765	.2820
0-2	H	2.71305	4.72322	0.5798	3.152	44.56	427416	245510	.2538
	L	2.66115				45.05	435751	245510	.2675
0-3	H	2.69664	4.68558	0.5794	3.1621	45.31	429720	247312	.2524
		2.65515				45.71	436435	247312	.2635
0-4	H	2.67089	4.71086	0.5796	3.1695	45.53	437294	246070	.2683
	L	2.65085				45.53	437294	246070	.2683
0-5	H	2.65684	4.76079	0.5796	3.1722	44.82	436308	243489	.2738
		2.64778				44.89	437801	243489	.2761
R-1	H	2.64806	4.62009	0.5797	3.1778	47.00	437830	250947	.2554
	L	2.64090				47.07	439017	250947	.2573
R-2	H	2.70202	4.73339	0.5796	3.1521	44.50	429012	244898	.2583
	L	2.65643				44.92	436375	244898	.2701
R-3	H	2.6643	4.69493	0.5795	3.1623	45.49	434664	246862	.2619
	L	2.64666				45.68	437910	246862	.2671
R-4	H	2.63531	4.64174	0.5800	3.1746	46.81	440176	249906	.2622
	L	2.62551				46.91	441919	249906	.2648
R-5	H	2.65650	4.63275	0.5801	3.1767	46.78	436740	250434	.2551
	L	2.65021				46.84	437777	250434	.2568

25

SAMPLE		Longitude Time	Shear Time	Thickness Inches	Density (gr/cm³)	Young's Modulus	longitude Velocity	Shear Velocity	Poissons Ratio
B-1	H	2.63741	4.75695	0.5799	3.1617	44.93	439750	243812	.2781
	L	2.62639				45.03	441595	243812	.2807
B-2	H	2.65294	4.75748	0.5797	3.166	44.82	437025	243700	.2744
	L	2.64576				44.89	438211	243700	.2761
B-3	H	2.66040	4.62381	0.5800	3.1679	46.72	436025	250875	.2526
	L	2.65530				46.77	436862	250875	.2540
B-4	H	2.63574	4.74581	0.5799	3.1715	45.25	440028	244384	.2770
	L	2.62125				45.37	442461	244384	.2805
B-5	H	2.64299	4.62263	0.5796	3.1702	46.88	438594	250766	.2572
	L	2.62327				47.08	441891	250766	.2625
W-1	H	2.65334	4.61107	0.5798	3.1778	47.09	437034	251482	.2525
	L	2.64445				47.18	438503	251482	.2550
W-2	H	2.62989	4.62447	0.5781	3.172	46.77	439638	250018	.2610
	L	2.61715				46.90	441778	250018	.2644
W-3	H	2.64495	4.74204	0.5799	3.193	45.53	438496	244578	.2742
	L	2.64231				45.55	438934	244578	.2749
W-	H	2.64279	4.74337	0.5800	3.1786	45.34	438930	24452	.2749
	L	2.63829				45.38	439679	244552	.2760
W-5	H	2.62492	4.58950	0.5757	3.1799	47.06	438642	250877	.2569
	L	2.60990				47.21	441166	250877	.2610
G-1	H	2.64739	4.64061	0.5792	3.1725	46.55	437563	249622	.2588
	L	2.64273				46.59	438335	249622	.2600
G-2	H	2.63970	4.75084	0.5799	3.1776	45.23	439368	244125	.8767
	L	2.62281				45.37	442197	244125	.2808
G-3	H	2.70314	4.79999	0.5793	3.1606	43.67	428613	241376	.2678
	L	2.65717				44.06	436028	241376	.2791
G-4	H	2.64776	4.73100	0.5798	3.1824	44.78	437955	242543	.2788
	L	2.63734				44.81	439685	242543	.2813
G-5	H	2.68196	4.67106	0.5797	3.1566	45.62	432296	248209	.2541
	L	2.65346				45.90	436939	248209	.2618

26

2.5.2 Reaction Bonded Silicon Nitride Flexure Specimens

The RBSN flexure speciemsn previously described were also subjected to nondestructive evaluation. A total of fifty-six beams were provided by Ford for both room and elevated temperature experiements. These specimens were porous ($\sim$75% theoretical density) and had obvious surface flaws on one face of the beam. Typical "C" scan observations are shown in Figure 9 for both sides of the samples. Apparently the lines correspond to the furnace rack supports used during the nitriding cycle. These are visually apparent on only one face and accordingly this poorer surface was used on the compression side during flexure.
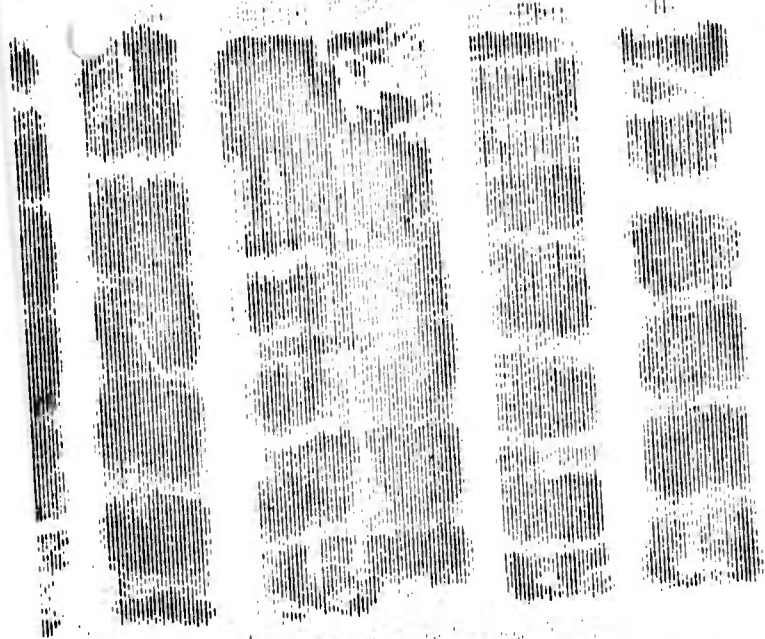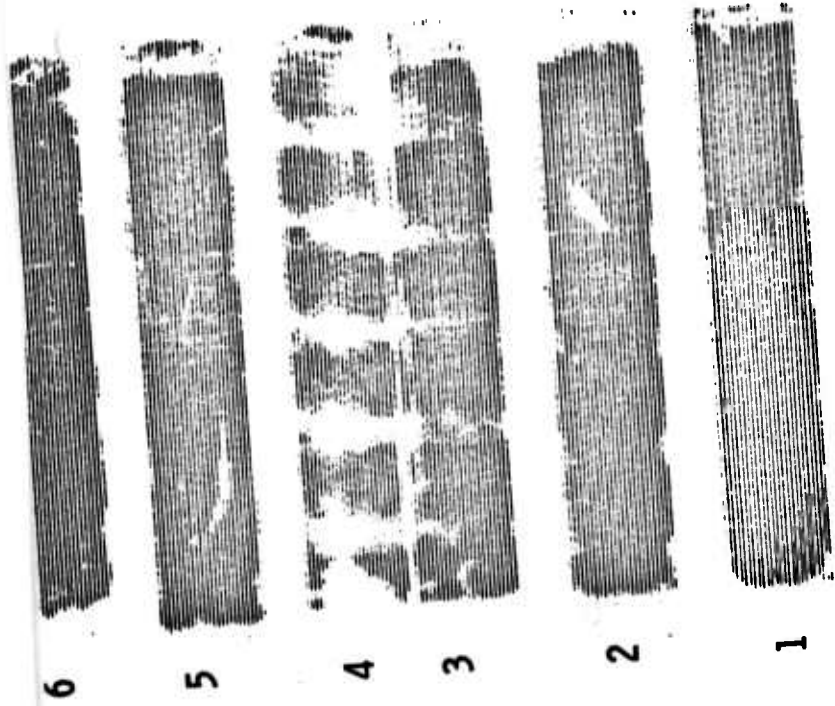
Specimens Reversed

15MHz - Panametrics Focused Transducer, HFN- 15 MHz Pulser Receiver, Index 3 3/4 , Scan S

Figure 9. Typical "C" Scan Observations, Flexure Specimens

28

2.5.3 ULTRASONIC VELOCITY MEASUREMENTS
ON
REACTION SINTERED SILICON NITRIDE STATORS

Two ceramic stators were subjected to ultrasonic examination.
Compression waves were introduced through both sides of the rim of the
stator wheel near the blade root area. Velocity transit times were
recorded for each location. At a later date these areas will be subjected
to mechanical testing and localized density measurements. The flexural
modulus and flexure strength will be determined using miniature beams
machined from the area of each blade root. Similar test will be
conducted on beams prepared from the individual stator blades. While
the strength measurements are not expected to be representative of actual
mechanical properties of the reaction sintered silicon nitride, the data
is expected to be representative of spatial variation of moduli and
strengths throughout these production parts. Note the data presented
in the following tables suggest high uniformity in modulus throughout
the parts.

TABLE 10   STATOR NUMBER 1

SITION	THICK. (IN)	TIME TL	TIME TS	Velocity VL in/sec	Velocity VS in/sec
A-1	.102	.682705	1.15093	298,811	177,248
A-2	.10	.679185	1.13017	294,471	176,965
A-3	.099	.668972	1.11757	295,977	177,170
A-4	.099	.661205	1.10182	299,453	179,703
A-5	.10	.661740	1.10764	302,234	180,564
A-6	.1005	.658878	1.10542	305,064	181,831
A-7	.10	.668772	1.12205	299,056	178,245
A-8	.1005	.674270	1.13099	298,100	177,720
A-9	.101	.677813	1.13287	298,017	178,308
A-10	.10105	.68880	1.13225	293,375	178,494
A-11	.102	.692256	1.15626	294,689	176,431
A-12	.1032	.696000	1.15955	296,552	178,000
A-13	.1034	.706389	1.17512	292,757	175,982
A-14	.1002	.705612	1.15071	284,009	174,153
A-15	.102	.703661	1.16426	289,912	175,219
A-16	.102	.704699	1.16945	289,485	174,441
A-17	.102	.707977	1.16647	288,145	174,887
A-18	.104	.703791	1.17261	295,542	177,382
A-19	.105	.686914	1.16992	305,715	179,449
A-20	.105	.689339	1.16745	304,640	179,879
A-21	.105	.688489	1.15258	305,016	182,200
A-22	.1035	.694473	1.16624	298,068	177,493
-23	.1025	.677188	1.14715	302,722	178,704
A-24	.102	.664549	1.120021	306,975	182,140
A-25	.101	.679029	1.15154	297,484	175,417
B-1	.103	.704320	1.18809	292,481	173,388
B-2	.103	.714875	1.20585	288,162	170,834
B-3	.103	.702683	1.17587	293,162	175,189
B-4	.103	.682249	1.15621	301,943	178,168
B-5	.1035	.687424	1.16393	301,124	177,846
B-6	.1025	.691121	1.16003	296,626	176,720
B-7	.102	.697800	1.9323	292,347	170,965
B-8	.1015	.694337	1.7737	292,365	172,418
B-9	.1013	.679722	1.15788	298,063	174,975
B-10	.0995	.683448	1.16884	291,171	170,254
B-11	.099	.659644	1.11760	300,162	177,165
B-12	.098	.669816	1.14853	294,111	171,524
B-13	.0976	.664173	1.15253	293,899	169,367
B-14	.0968	.666322	1.162011	290,550	166,608
B-15	.097	.658538	1.11898	294,592	173,372
B-16	.0968	.632487	1.10686	306,093	174,909
B-17					
B-18					
B-19	.097	.659145	1.11735	294,321	173,539
B-20	.098	.674405	1.13608	290,627	172,523
B-21	.099	.677398	1.16048	292,295	170,619
-22	.099	.681805	1.16258	290,406	170,311
B-23	.10	.682806	1.16923	292,909	171,053
B-24	.1012	.692123	1.19066	292,434	169,990
B-25	.1016	.674874	1.16322	301,093	174,688

30

	PARTS	THICK. (IN)	LONG	SHEAR	V_L in/sec	V_S in/sec
			Microseconds			
	C-1	.257	1.56574	2.68215	328.279	191,637
Notch	C-2	.249	1.56734	2.75043	317,735	181,063
	C 3	.252	1.55490	2.79278	324,137	180,465
High Att.	C-4	.2475	1.53038		323,449	
	C-5	.250	1.52177	2.62011	328,565	190,832
	C-6	.247	1.52132	2.60980	324,718	189,287
	C-7	.251	1,55483	2.66285	322,864	188,520
	C-8	.251	1,53662	2.64056	326,691	190,111
	C-9	.2475	1,53849	2.65446	321,744	186,479
	C-10	.247	1,54184	2.65211	320,396	186,267
High Att.	C-11	.252	1,55776	2.70057	323,541	186,627
	C-12	.2413	1,53291	2.62459	314,826	183,876
	D-1	.1975	1,20977	2.06419	326,508	191,358
	D-2	.197	1,21678	2.08911	323,805	188,597
	D-3	.202	1,22440	2.12636	329,958	189,996
	D-4	.205	1,27909	2.16658	320,540	189,238
	D-5	.204	1,24884	2.15082	326,703	189,695
	D-6	.204	1,25778	2.14086	324,381	190,578
	D-7	.1965	1,21106	2.08497	324,509	188,492
	D-8	.198	1.21971	2.08298	324,667	190,112
	D-9	.200	1.22976	2.08813	325,267	191,559
	D-10	.2015	1,21832	2.13440	330,783	188,812
	D-11	.1965	1.21622	2.07586	323,132	189,319
	D-12	.203	1.23816	2.11275	327,906	192,167

TABLE 11   STATOR NUMBER 2

3.0 PROBABILITY BASED DESIGN & ANALYSIS

The basic idea of probability based design and analysis is to attempt to design a specified reliability directly into a component, rather than to use a conventional safety factor approach which is based merely on average values of strengths and mean load conditions. Benefits of the approach include the ability to assess the sensitivity of the design to variability in material properties, mechanical and thermal loads, geometric tolerances, etc. Furthermore the probabilistic approach provides an estimate of failure rates of the components of the design, under expected service conditions.

There are a variety of methods to incorporate statistical considerations into stress analysis. In this report, we begin first with determination of appropriate statistical models to represent the strength behavior of the ceramics. In particular the room temperature tensile strength of hot pressed silicon nitride is used in determining suitability of various simple models.

WEIBULL DISTRIBUTION

Consider a material which, under a uniform stress condition, has the probability of failure of P_f per unit volume. Then the overall probability of survival for volume V of the material is given by

$$P_s = (1-P_f)^V$$

for the simultaneous survival of V volume units. Then

$$\ln S = V \ln (1-P_f)$$

Weibull statistics (3) defines the risk of rupture as $R = -\ln S$ and in terms of an infinitesimal element, gives

$$dR = -\ln(1-P_f) \, dV$$

where the term $-\ln(1-P_f)$ is assumed to be a positive function, $n(\sigma)$ of the tensile stress σ, alone. Substitution gives $dR = n(\sigma)\ dV$

$$R = \int_V n(\sigma)\ dv$$

From this definition of R we arrive at

$$P_s = \exp\left[-\int_V n(\sigma) dV\right]$$

Several forms for $n(\sigma)$ were proposed by Weibull, e.g.

$$n(\sigma) = \left(\frac{\sigma}{\sigma_o}\right)^m$$

$$n(\sigma) = \left(\frac{\sigma-\sigma_u}{\sigma_o}\right)^m$$

and in these cases

$$P_s = \exp\left[-\int_V \left(\frac{\sigma}{\sigma_o}\right)^m dV\right]$$

$$P_s = \exp\left[-\int_V \left(\frac{\sigma-\sigma_u}{\sigma_o}\right)^m dV\right]$$

Another form was proposed(4) to account for a maximum value of stress, above which the probability of survival vanishes

$$n(\sigma) = \left(\frac{\sigma-\sigma_u}{\sigma_s-\sigma}\right)^m$$

where

$$n(\sigma) \equiv 0 \qquad \sigma < \sigma_u, \quad \sigma > \sigma_s$$

EFFECT OF SIZE AND STRESS DISTRIBUTION

Using the simplest form of $n(\sigma)$, if we compare two types of specimens under uniform stress states at the same value of failure probability then the ratio of stresses for the two volumes is

$$\frac{\sigma_1}{\sigma_2} = \left(\frac{V_2}{V_1}\right)^{1/m}$$

Strength is therefore shown dependent on volume and decreases as the volume increases. Furthermore the effect becomes less important as the value of the "Weibull" modulus m increases. The equation can be generalized in the form $\exp\left[KVn(\sigma)\right]$ where K is a normalized geometry integral and σ is a reference stress state. For the same type of test specimens, the size effect will be as

33

theoretically defined. Thus by performing experiments on various sizes of specimens and also by using different types of loadings, it is possible to compare and assess the applicability of such representations for observed material strengths. First, however, we begin by apply ng several of the more common methods to fit Weibull models to experimental data.

3.1 EVALUATION OF WEIBULL PARAMETERS

1.1.1 THEORETICAL CURVE FITTING METHODS

METHOD OF MOMENTS - Three Parameter Weibull

The method of moments is based on choosing the Weibull parameters

i.e. $$m, \ \sigma_o, \ \sigma_u$$

so that the first three moments of the distribution correspond to those of the observed data. The first step is to calculate these 3 moments from the data. Let us label these as

σ_m = Mean strength

a^2 = Square of the standard deviation

μ = Third moment about the mean

Furthermore, let N = Number of datapoints and,

σ_m = The strength of the "n" specimen

Then the first moment

$$\sigma_m = \frac{1}{N} \sum_{m=1}^{N} \sigma_m \tag{1}$$

Second moment

$$a^2 = \frac{1}{N} \sum_{m=1}^{N} (\sigma_m - \sigma_m)^2 \tag{2}$$

Third moment

$$\mu = \frac{1}{N} \sum_{m=1}^{N} (\sigma_m - \sigma_m)^3 \tag{3}$$

Consideration of the theoretical distribution and taking the corresponding moments of all points on the probability curve about the smallest point σ_u leads to the following theoretical relations

$$\sigma_m = \sigma_u + \frac{\sigma_o}{(KV)^{1/m}} \Gamma\left(1+\frac{1}{m}\right) \tag{4}$$

where KV is the appropriate constant K and Volume V for the particular type of test specimen and $\Gamma\left(1+\frac{1}{m}\right)$ is the Gamma Function. Furthermore

$$a^2 = \frac{\sigma_o^2}{(KV)^{\frac{2}{m}}} \left[\Gamma\left(1+\frac{2}{m}\right) - \Gamma^2\left(1+\frac{1}{m}\right)\right] \tag{5}$$

$$\mu = \frac{\sigma_o^3}{(KV)^{\frac{3}{m}}} \left[\Gamma\left(1+\frac{3}{m}\right) - 3\Gamma\left(1+\frac{2}{m}\right)\Gamma\left(1+\frac{1}{m}\right) + 2\Gamma^3\left(1+\frac{1}{m}\right)\right] \tag{6}$$

These equations could be solved by trial procedures for m, σ_o, σ_u. However this would be cumbersome. Instead by dividing equation (6) by (5) raised to 3/2 power we define

$$A_3 = \frac{\mu}{(a^2)^{3/2}}$$

(which can be computed from the data)

$$A_3 = \frac{\Gamma\left(1+\frac{3}{m}\right) - 3\Gamma\left(1+\frac{2}{m}\right)\Gamma\left(1+\frac{1}{m}\right) + 2\Gamma^3\left(1+\frac{1}{m}\right)}{\left[\Gamma\left(1+\frac{2}{m}\right) - \Gamma^2\left(1+\frac{1}{m}\right)\right]^{3/2}} \tag{7}$$

This new "variable" A_3 can therefore be calculated as a function of Weibull parameter m. Either a graphical procedure or a computer search technique can be used therefore to estimate the value of m which corresponds to the calculated A_3.

Now by rearranging equation (5) we can also define

$$A_2 = \frac{a^2 (KV)^{2/m}}{\sigma_0^2} = \left[\Gamma\left(1 + \frac{2}{m}\right) - \Gamma^2\left(1 + \frac{1}{m}\right) \right] \qquad (8)$$

and now A_2 may be calculated using the value of m estimated via A_3
Then since $a^2 (KV)^{\frac{2}{m}}$ is a known quantity, σ_0^2 is calculated from
equation (8). Finally let $A_1 = \Gamma\left(1 + \frac{1}{m}\right)$

then we can rewrite (4)

$$\sigma_u = \sigma_m - \frac{\sigma_0 A_1}{(KV)^{1/m}}$$

These equations have been programmed and iterative procedures adopted
to apply this technique. Examples of the method appear next.

TABLE 12

EVALUATION OF PARAMETERS BY METHOD OF MOMENTS

HOT PRESSED SILICON NITRIDE

Strength σ_n, Ksi	σ_n^2	σ_n^3
85.41	7294.87	623,054.68
78.77	6204.71	488,745.23
76.77	5893.63	452,454.20
73.54	5408.13	397,714.00
69.820	4874.83	340,360.80
65.46	42851.01	280,496.9
65.39	4275.85	279,597.97
63.62	4047.5	257,502.23
63.02	3971.52	250,285.21
62.88	3953.89	248,620.88
61.82	3821.71	236,258.26
54.70	2992.09	163,667.32
52.67	2774.13	146,113.37

Mean strength $\quad \sigma_m = \dfrac{1}{N} \sum \sigma_m \quad = 67{,}221$

Square of Standard Deviation

$$a^2 = \frac{1}{N} \sum \left(\sigma_m - \sigma_m \right)^2 = 83.2 \text{ Ksi}^2$$

38

TABLE 13

Standard Deviation

σ_m	$\sigma_m - \bar{\sigma}_m$	$(\sigma_m - \bar{\sigma}_m)^2$
85.41	18.189	330.84
78.77	11.549	133.3794
75.77	9.549	91.1834
73.54	6.319	39.9298
69.82	2.599	6.7548
65.46	1.761	3.101121
65.39	1.831	3.352561
63.62	3.601	12.9672
63.02	4.201	17.6484
62.88	4.341	18.84428
61.82	5.401	29.1708
54.7	13.151	172.9488
52.67	14.551	221.7316

$$a^2 = \tfrac{1}{13}(1081.852163) = 83.2194$$

39

Third Moment

$$M = \frac{1}{N} \sum \sigma_m^3 - 3 \frac{\sigma_m}{N} \sum \sigma_m^2 + 2(\sigma_m)^3$$

$$M = 256 \times 10^9$$

$$A_3 = \frac{M}{(a^2)^{3/2}} = .337$$

and $m \simeq 2.6$

$$A_2 \simeq .135$$

$$\sigma_o = 7491$$

$$A_1 \simeq .887$$
$$\sigma_u = 45,198$$

and supposedly the probability of failure

$$P_f = 1 - exp\left[-.0471 \left(\frac{\sigma - 45,198}{7491}\right)^{2.25}\right]$$

3.1.2 GRAPHICAL PROCEDURES

The starting three parameter equation can be written as

$$\frac{1}{1-P_f} = \exp KV\left(\frac{\sigma-\sigma_u}{\sigma_o}\right)^m$$

or taking logarithims

$$\ln\ln\left(\frac{1}{1-P_f}\right) = m\ln(\sigma-\sigma_u) + \ln\left(\frac{KV}{\sigma_o^m}\right)$$

Now theoretically the statisfical distribution function will be linear if the data is plotted on coordinates $\ln\ln\left(1-\frac{1}{P_f}\right)$ versus $\ln(\sigma-\sigma_u)$ and the slope of the linear curve will yield the Weibull modulus m.

An example of evaluation of the Weibull parameters is presented next:

TABLE 14

Rank	Probability of Failure $\frac{n}{N+1}$	$\ln\ln(\frac{N+1}{N+1-n})$	Strength psi	Two Parameter Distribution $\ln \sigma$	Three Parameter $\ln (\sigma - \sigma_u)$
1	.07143	-2.602	52,670	10.8718	8.9189
2	.1429	-1.870	54,700	10.9096	9.1593
3	.2143	-1.422	61,820	11.03198	9.7185
4	.2857	-1.089	62,880	11.04898	9.7803
5	.357	-0.817	63,020	11.0512	9.7882
6	.4286	-0.580	63,620	11.0607	9.8213
7	.500	-0.366	65,390	11.0881	9.9130
8	.5714	-0.165	65,460	11.0892	9.9165
9	.6429	0.0292	69,820	11.1537	10.1114
10	.7143	0.225	73,540	11.2056	10.2521
11	.7857	0.432	76,770	11.2486	10.3600
12	.857	0.666	78,770	11.2743	10.4215
13	.9287	0.970	85,410	11.3552	10.6019

Note that the value σ_u = 45,198 was obtained previously by the method of moments. Otherwise a trial procedure would have been employed to arrive at value of σ_u.

42

The data for the two and three parameter distribution are shown in Figure 10 Comparison of the graphical procedure and the method of moment models is made in Figure 11. It is apparent that there is a certain amount of flexibility in fitting the rather limited data; and several models could justifiably be chosen to represent the measurements.

NORMALIZED STRESS METHOD

In this method (6) the equations suggested by Weibull are rewritten with the mean strength σ_m substituted for σ_o and $\sigma_u = 0$. Then Ps can be written as

$$P_s = \exp -\left[\left(\beta\, \Gamma\left(1 + \tfrac{1}{m}\right)\right)\right]^m$$

where $\beta = \dfrac{\sigma}{\sigma_m}$ and σ is the failure stress associated with a particular probability of survival P_s.

The procedure for evaluation of a set of data by this method is to normalize the observations by dividing by the mean strength and rank these in order of increasing size. As examples of the method, the normalized strength, β, and corresponding probability of survival values are tabulated for tension and flexure data on HPSN and flexure data for RBSN. The values are plotted in Figures 12, 13. Note that in the region β near 1.0 a small uncertainty is probability results in a wide band of m values. If the data tend to a vertical line then a single two parameter Weibull distribution describes the data. This is apparently not the case for the test results reported here. (See Figure 12).
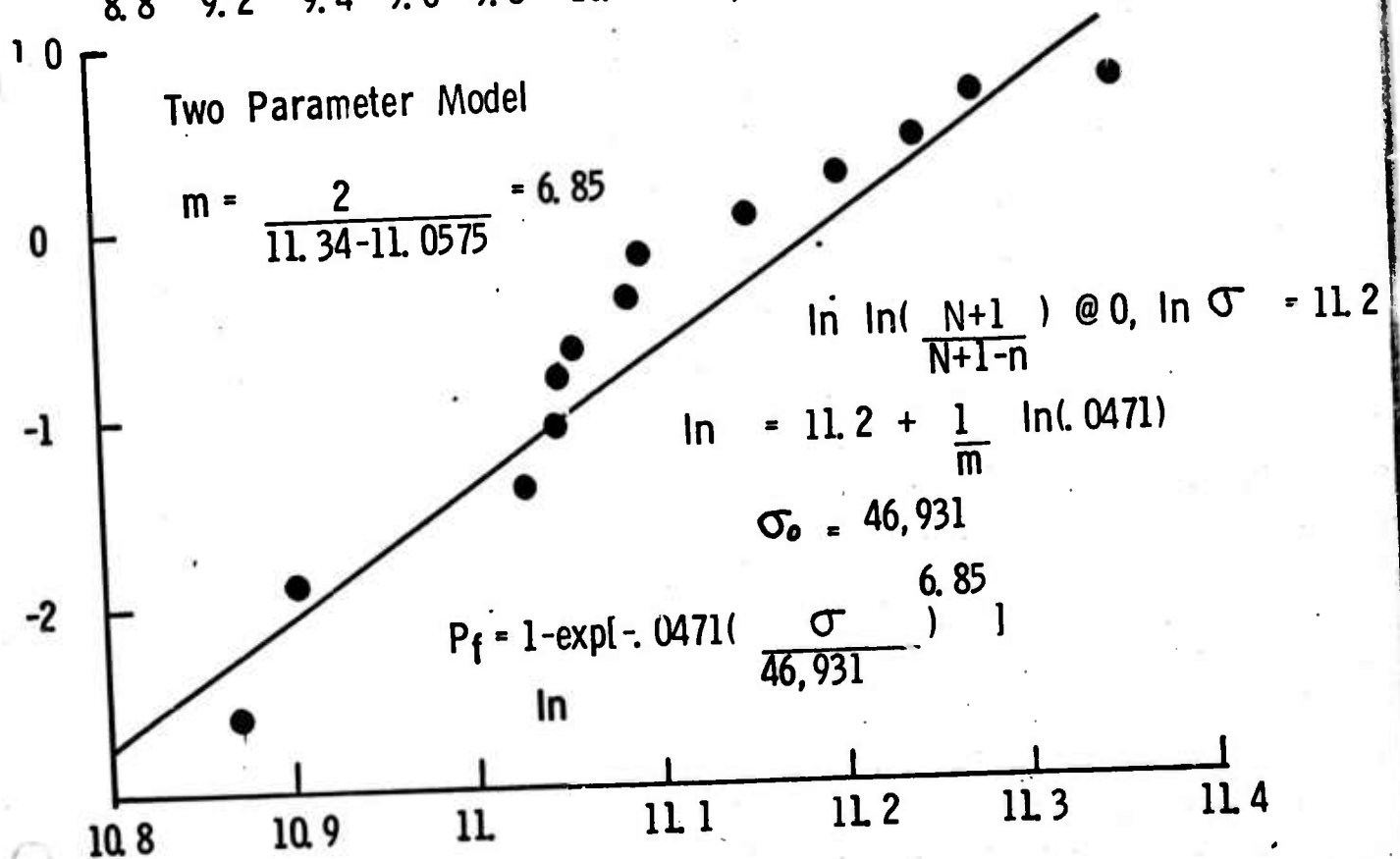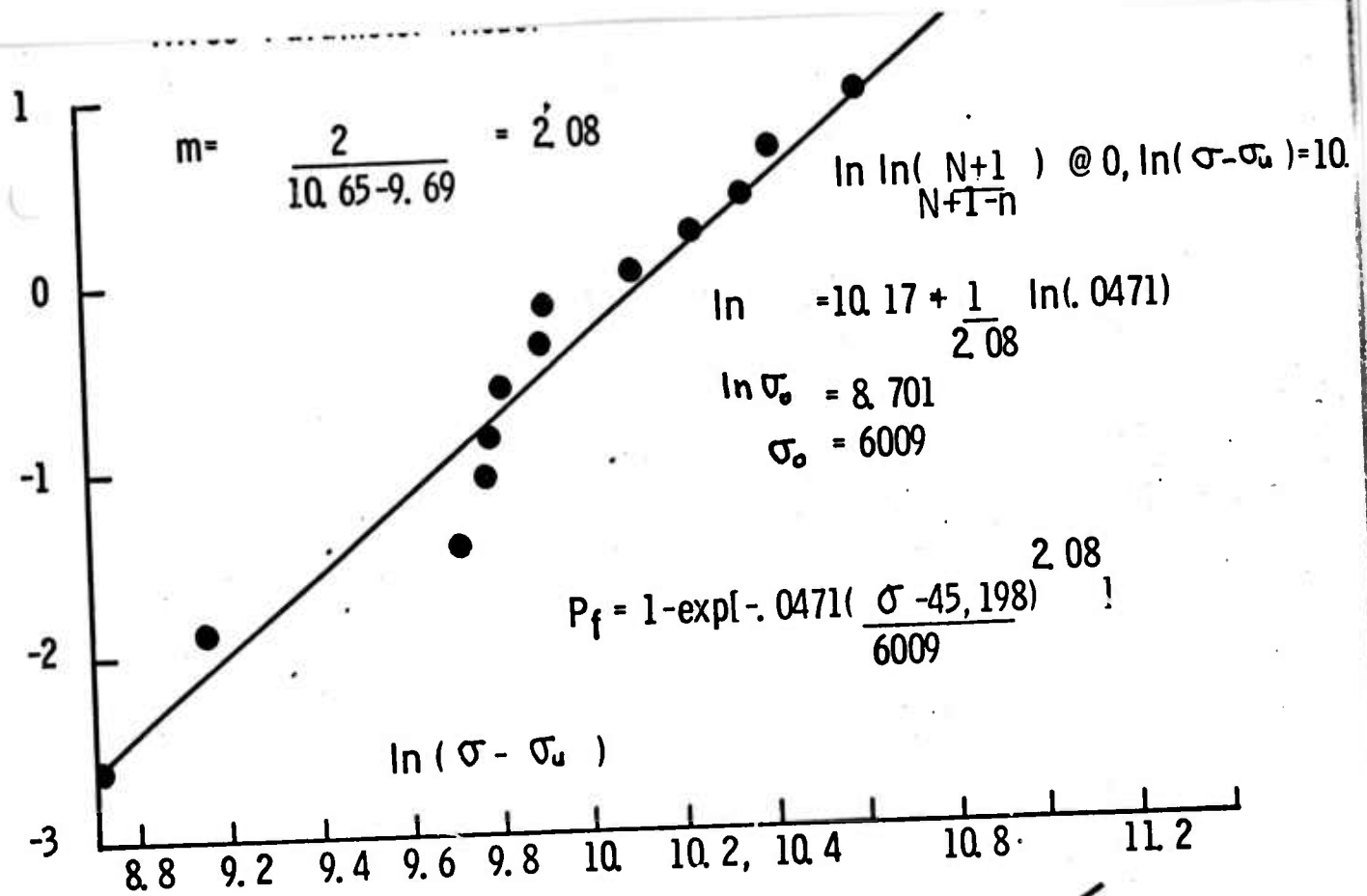
43

Three Parameter Model

$$m = \frac{2}{10.65 - 9.69} = 2.08$$

$\ln \ln \left(\frac{N+1}{N+1-n} \right)$ @ 0, $\ln (\sigma - \sigma_u) = 10.$

$$\ln = 10.17 + \frac{1}{2.08} \ln(.0471)$$

$$\ln \sigma_o = 8.701$$

$$\sigma_o = 6009$$

$$P_f = 1 - \exp\left[-.0471 \left(\frac{\sigma - 45,198}{6009} \right)^{2.08} \right]$$

$\ln (\sigma - \sigma_u)$

Two Parameter Model

$$m = \frac{2}{11.34 - 11.0575} = 6.85$$

$\ln \ln \left(\frac{N+1}{N+1-n} \right)$ @ 0, $\ln \sigma = 11.2$

$$\ln = 11.2 + \frac{1}{m} \ln(.0471)$$

$$\sigma_o = 46,931$$

$$P_f = 1 - \exp\left[-.0471 \left(\frac{\sigma}{46,931} \right)^{6.85} \right]$$

$\ln$

Figure 10. Graphical Fits of Tension Data to Two and Three Parameter Model

44
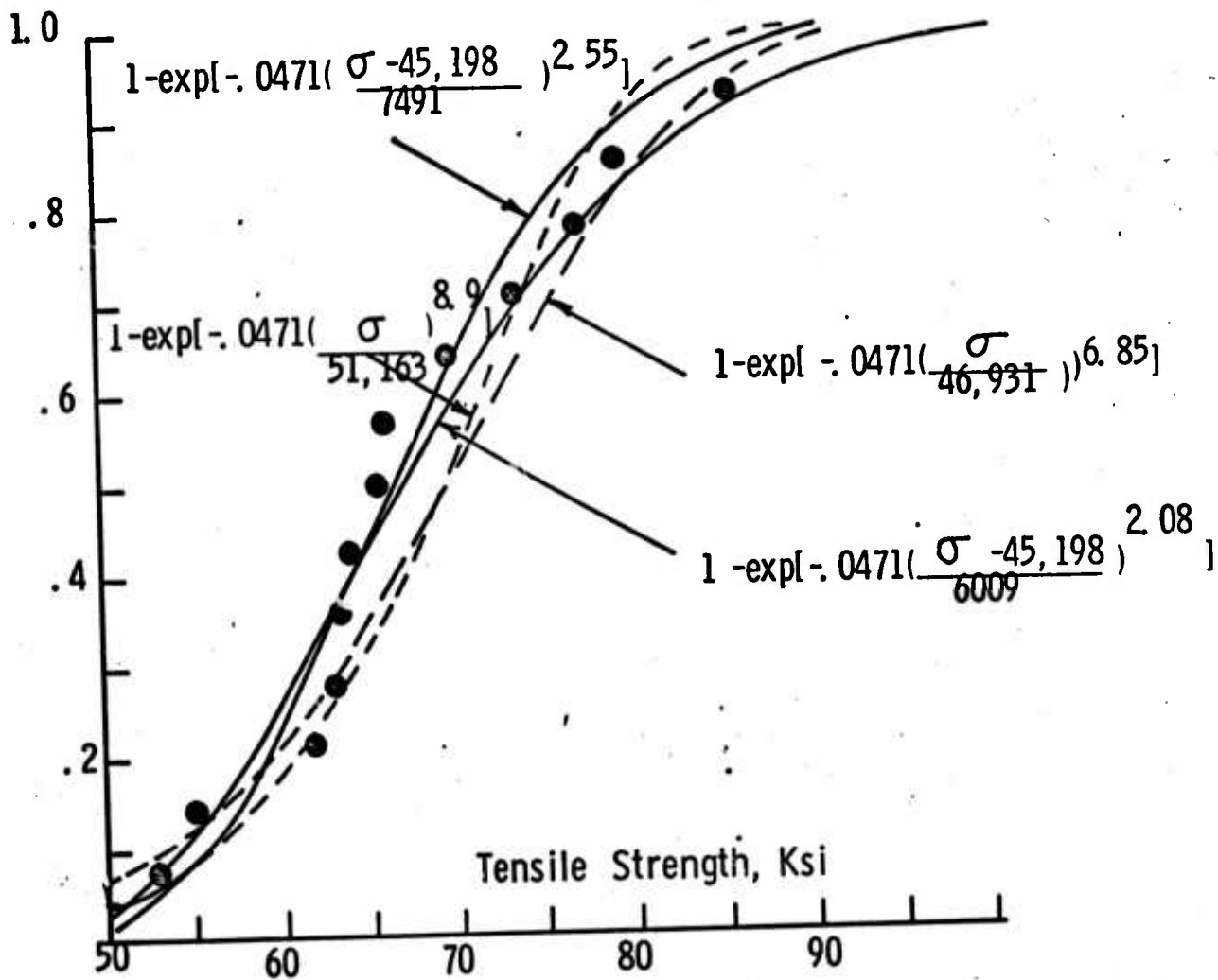
Figure 11. Comparison of Various Weibull Models to Tension Data

45

TABLE 15   TENSION STRENGTH, HPSN

Rank R	Strength	Probability	$\beta = \dfrac{\sigma_i}{\sigma_m}$	$\dfrac{R-.3}{N+.4}$
1	52,670	.077	.784	.948
2	54,700	.154	.815	.873
3	61,820	.231	.922	.798
4	62,080	.308	.938	.724
5	63,020	.385	.942	.650
6	63,620	.462	.947	.575
7	65,390	.538	.973	.500
8	65,460	.615	.976	.425
9	69,820	.692	1.04	.35
10	73,540	.770	1.097	.277
11	76,770	.846	1.142	.200
12	78,770	.923	1.17	.127
13	85,410	1.00	1.27	.052

N = 13   mean = 67,200

Refer to Figure 12, and disregarding three lowest values, m = 8.94

TABLE 16 FLEXURE STRENGTH, HPSN

Rank R	Strength	β	$\dfrac{R-.3}{N+.4}$
1	72,722	.764	.95
2	74,467	.778	.9023
3	82,778	.870	.845
4	85,111	.895	.787
5	95,277	1.0	.73
6	95,556	1.001	.673
7	95,833	-	.615
8	96,444	1.012	.557
9	97,222	1.02	.500
10	98,889	1.037	.442
11	100,000	1.05	.385
12	100,722	1.125	.327
13	101,389	1.062	.270
14	103,194	1.085	.214
15	106,667	1.117	.155
16	107,611	1.13	.098
17	109,444	1.15	.022

N = 17

mean = 95,443

Disgarding values near B = 1, then from Figure 12, m = 10.6

TABLE 17   FLEXURE TESTS ON RBSN

Strength	Rank	$1 - \dfrac{R-.3}{N+.4}$	β
11,444	1	.9513	.77
12,444	2	.882	.835
13,556	3	.812	.91
14,4667	4	.743	.984
14,778	5	.673	.99
14,778	6	.613	.99
15,111	7	.535	1.013
1533	8	.465	1.03
15,556	9	.398	1.042
15,611	10	.327	1.047
16,000	11	.257	1.073
16,111	12	.188	1.082
16,556	13	.118	1.11
16,889	14	.048	1.132

mean = 14,917

and from Figure 12, m = 14.3
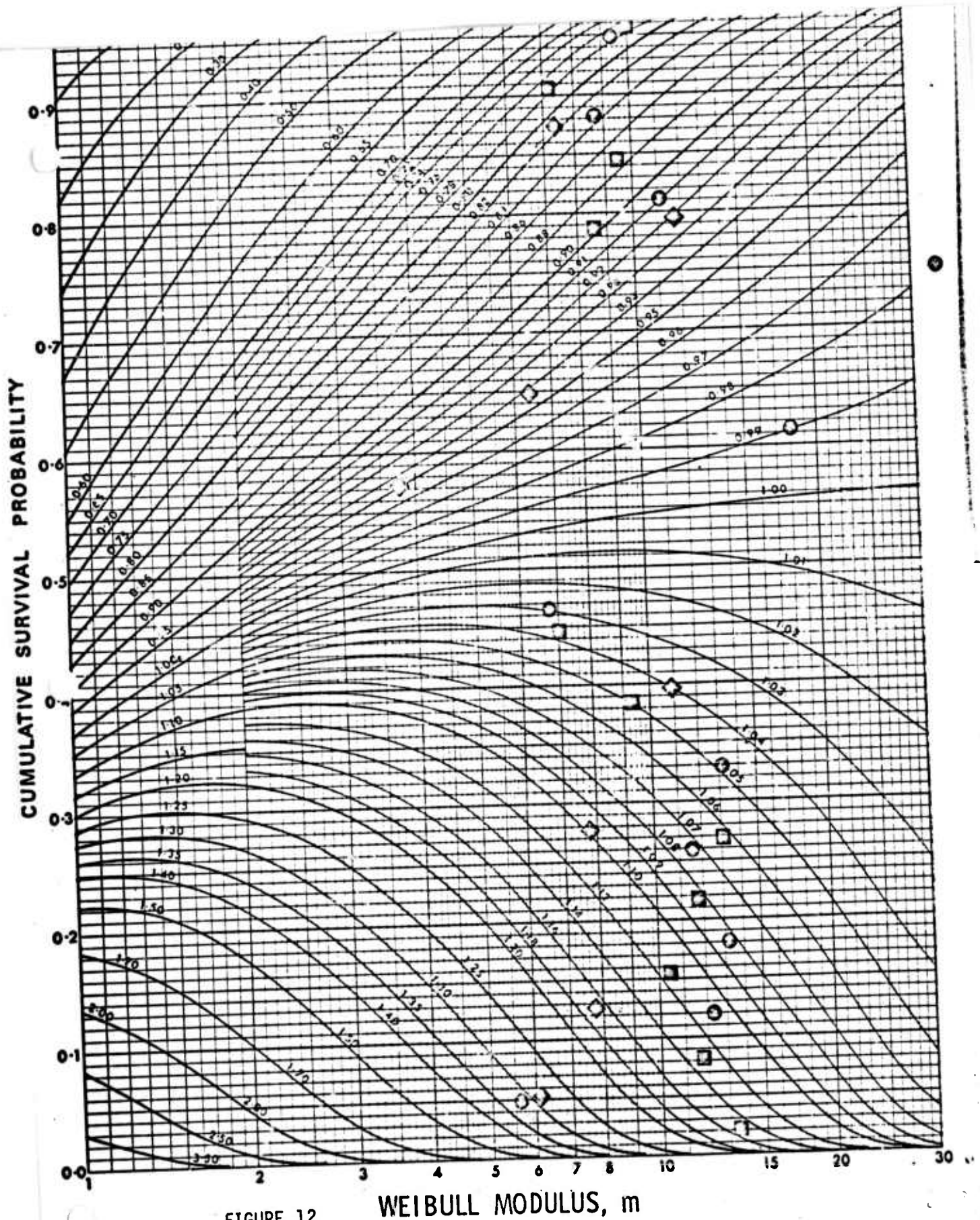
FIGURE 12

Tension, HPSN ◆
Flexure, HPSN ■   RBSN ●   Plotting Position $1 - \dfrac{R - .3}{N + .4}$, $\beta = \dfrac{\sigma_N}{\sigma_{average}}$

49

There are a number of alternate approaches to describe the results
if the data are curved about either side of a vertical distribution.
First the three paramter distribution might better represent the data.
Alternatively a combination of two parameter distributions might better
fit the measurements. In the case of the three parameter distribution,
β is defined as $\dfrac{\sigma - \sigma_u}{\sigma_m - \sigma_u}$. The tension strengths for HPSN
are evaluated this way in the following tabulation and in Figure [13].
The value of σ_u determined via the method of moments is chosen to treat
the data, e.g. σ_u = 45,198

TABLE 18

Rank	σ_i	β	$1 - \dfrac{R-.3}{N+.4}$
1	52,670	.3393	.948
2	54,700	.4315	.873
3	61,820	.7548	.798
4	62,880	.8029	.724
5	63,020	.80924	.65
6	63,620	.8345	.575
7	65,390	.9169	.5
8	69,460	.920	.425
9	69,820	1.118	.35
10	73,540	1.287	.277
11	76,770	1.434	.2
12	78,770	1.524	.127
13	85,410	1.826	.052

N = 13

and the range in m from Figure 13 is 1.2 to 3.8
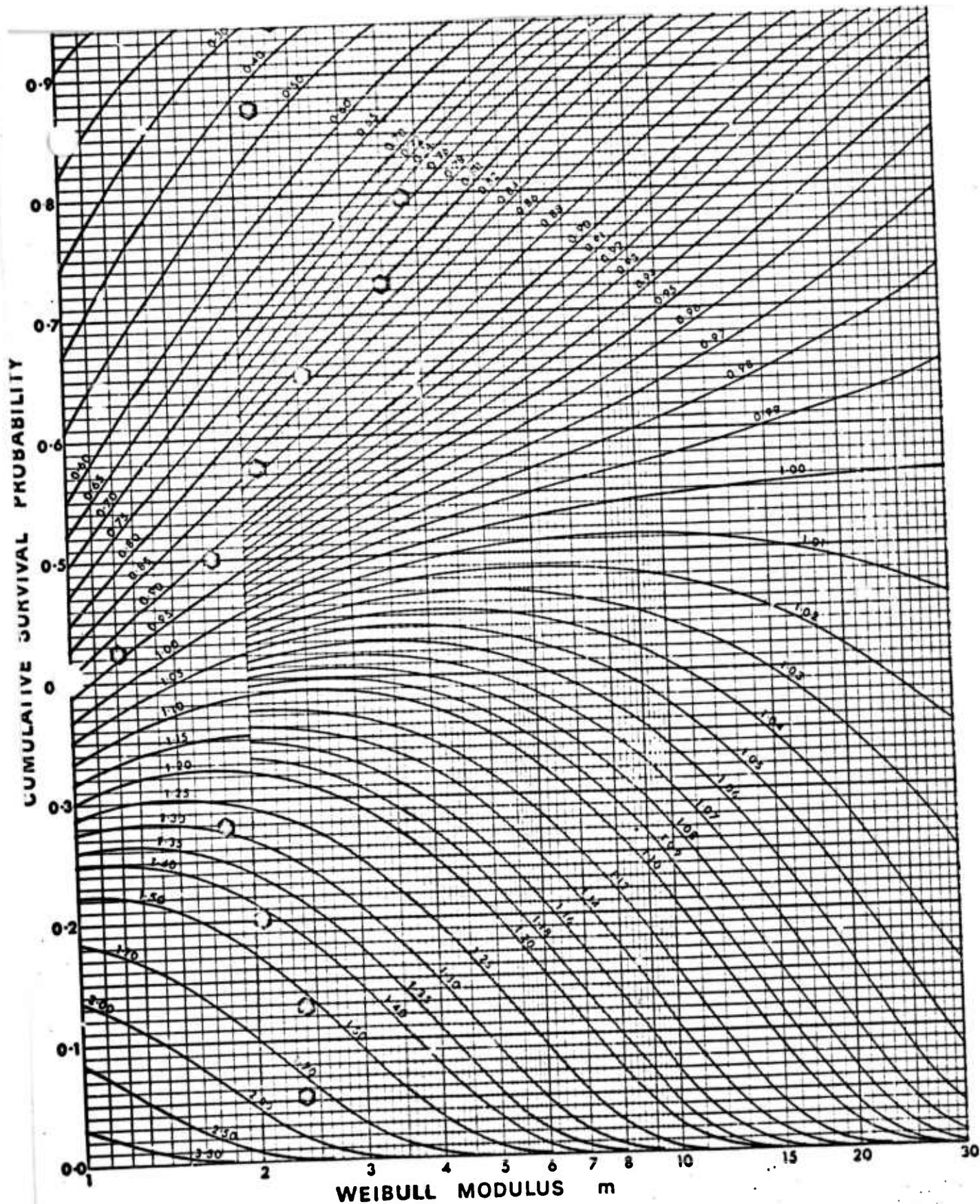
Figure 13. Normalized Three Parameter Weibull Distribution
51
Tensile Data

From the preceding discussion, it appears that for the rather small sample sizes used here, the normalized stress method is not useful for values near $\beta = 1$. Other, and simpler model fitting techniques are advisable. It is interesting, however to compare the results obtained from the different techniques just discussed.

TABLE 19   SUMMARY OF WEIBULL PARAMETERS
OBTAINED BY VARIOUS TECHNIQUES

Technique	Two Parameter Model			Three Parameter Model	
Method of Moments	51,163	8.9	7491	45,198	2.55
Graphical	46,931	6.85	6009	45,198	2.08
Normalized Distribution	-	8.94			2.34

From the earlier discussion we have that Mean Failure

Strength $\sigma_m = \sigma_u + \int_{\sigma_u}^{\infty} \exp^{-R} d\sigma$

Variance $\delta^2 = \int_{\sigma_u}^{\infty} \exp^{-R} d(\sigma^2) + \sigma_u^2 - \sigma_m^2$

and the risk of rupture

$R = \int_V \left(\frac{\sigma - \sigma_u}{\sigma_0} \right)^m dV$

Supposedly the three distribution parameters m, σ_o and σ_u are independent of size and manner of loading and in general

$$R = KV\left(\frac{\sigma - \sigma_u}{\sigma_o}\right)^m$$

where the load factors have been presented for simple mechanical tests by a number of authors (6,7).

For a two parameter model, the mean failure strength

$$\sigma_m = \sigma_o \frac{\Gamma\left(1 + \frac{1}{m}\right)}{(KV)^{1/m}}$$

and

$$S^2 = \frac{\sigma_o}{(KV)^{2/m}}\left[\Gamma\left(1 + \frac{2}{m}\right) - \Gamma^2\left(1 + \frac{1}{m}\right)\right]$$

and under simple tension K the loading factor becomes 1.0. Figure 14 shows the estimated mean strength volume dependency for HPSN in comparison to test data. Considering data variability the models appear reasonably consistent. When additional data is available the analytical expressions will be further refined and surface, as opposed to volume dependency will also be surveyed.
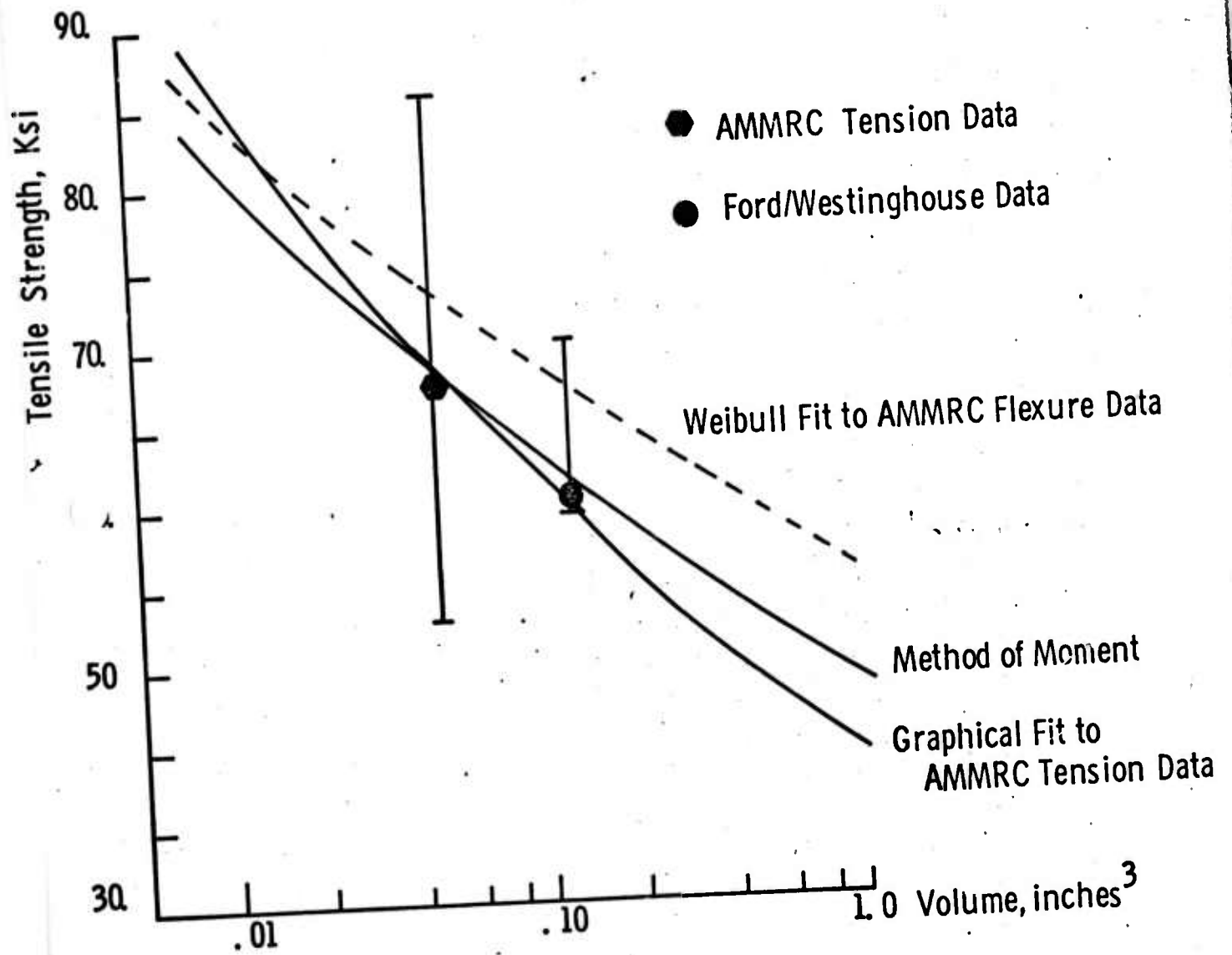
Figure 14. Tensile Strength versus Volume, Hot Pressed Silicon Nitride, Norton HS 130

54

3.2 Choice of the Probability Model

Suppose the test specimens could be assumed representative of the production parts in all respects, including the surface machining. Then our test data can be assumed to represent statistical variation of the material properties and there remains the question of choosing the appropriate statistical model to fit the data.

Quite often, for instance, material strength properties are taken to have normally distributed properties (8). Given the fact that test data is ordinarily too limited in quantity, and this does not allow a precise theoretical discrimination between various analytical models, the actual statistical model is often selected on the basis of convenience.

Reliability theories have been fairly extensively developed for normal, log-normal, two and three parameter Weibull and other statistical distributions. Each distribution has unique qualities and can be applied in various ways.

Thus unless there are firm theoretical basis for choosing one particular distribution, the selection is made after applying simple goodness of fit criteria and ease of use of the data. The normal distribution, for instance is easily applied to simple design formula. Haugen (9) has discussed two parameter, statistical algebra wherein elementary reliability calculations are stated in terms of mean values and standard durations of the variables. However, before discussing methods of applying other distributions, let us consider several of the properties of the Weibull distribution.

RELATIONSHIP BETWEEN PROBABILITY BASED STRENGTH

AND

FACTOR OF SAFETY

Suppose the material strength can be represented as a two parameter

Weibull distribution then the Probability of Survival, P_S is given by

$$P_S = 1 - P_F = \exp\left[-KV\left(\frac{\sigma}{\sigma_0}\right)^m\right]$$

$$\text{or } P_S = \exp\left[-\frac{\sigma}{\sigma_m}\Gamma\left(1+\frac{1}{m}\right)\right]^m$$

with σ = applied stress

σ_m = mean strength

Then let $SF = \dfrac{\sigma_m}{\sigma}$ = conventional safety factor

and in effect this previous equation is a relation between probability

safety factor and Weibull modulus, m.

The safety factor, SF, can also be expressed as

$$SF = \frac{\sigma_m}{\sigma} \quad \frac{\Gamma\left(1+\frac{1}{m}\right)}{\left[\ln\left(\frac{1}{P_S}\right)\right]^{1/m}}$$

in which for high reliability levels, the approximations

$$\ln\left(\frac{1}{P_S}\right) = P_F + \left(\frac{P_F}{2}\right)^2 + \cdots \simeq P \text{ for } P_F < 10^{-3}$$

$$P_F = 1 - P_S$$

Then $\quad SF \simeq \quad \left(\frac{1}{P_F}\right)^{1/m}$

and since $\quad \Gamma\left(1+\frac{1}{m}\right) \simeq 1 \text{ for most values of m}$

$$P_F \simeq \left(\frac{\sigma}{\sigma_m}\right)^m$$

Now if a structure is composed of m subvolumes, each with a volume equal to that of the test specimen, or alternatively using the appropriate Weibull parameters then the safety factor for the array of subvolumes under uniform stress σ is

$$S_F = \frac{\sigma_m}{\sigma} = \frac{(m)^{1/m} \, \Gamma\left(1 + \frac{1}{m}\right)}{\ln\left(\frac{1}{P_s}\right)^{1/m}} \simeq \left(\frac{m}{P_f}\right)^{1/m}$$

or

$$P_f = 1 - P_s \simeq m \left(\frac{\sigma}{\sigma_m}\right)^m$$

The extreme safety factor SF_{min} is also of interest. This is defined as the ratio of the probable least strength of the material $\overline{\sigma_m}$ to the probable design stress σ_D

$$SF_{min} = \frac{\overline{\sigma_m}}{\sigma_D}$$

Using analytical methods, we can predict the most likely least value in a set of m specimens (10). In particular the probability of m specimens simultaneously surviving the stress σ is given by

$$P_{s_m} = \left[P_s(\sigma)\right]^m$$

Probability density is found by d fferentiating once e.g.

$$\frac{d P_{s_m}}{d\beta_m} = m \, P_s^{m-1} \frac{d P_s}{d\beta}$$

$$\beta = \frac{\sigma}{\sigma_m}$$

The most probable least value corresponds to the maximum of the probability density which is obtained by another differentiation and equating to zero. This yields

$$(m-1)\left(\frac{d P_s}{d\beta}\right)^2 = -\frac{d^2(P_s)}{d\beta} P_s$$

57

Using the two parameter Weibull expression leasts to the most likely
least value

$$\beta^* = \frac{\overline{\sigma_m}}{\sigma_m} = \left(\frac{m-1}{m\,m}\right)^{1/m} \frac{1}{\Gamma\left(1+\frac{1}{m}\right)}$$

From these elementary considerations, it is apparent that the Weibull
distribution permits a variety of useful generalizations and a formal
approach particularly suited for rapid assessment of reliability in
structures under simple stress conditions and where the variability
in loading is not large, so that predominant statistical variation is due
to strength as opposed to applied stresses.

3.3 APPROACHES FOR PROBABILITY BASED STRESS ANALYSIS

Suppose we are dealing with a material which does not exhibit volume dependent strength. Furthermore assume that no variation in the critical mechanical and thermal loadings is expected. Let the probability density distribution of strength be

$$\sigma(s)$$

Let the probability density distribution function associated with the applied stresses throughout the structure and resulting from the design load be

$$\sigma(\mathcal{A})$$

Then the reliability i.e. the conditional numerical probability that the component will perform without failure may be formally stated as

$$\text{Reliability} = R = \int_{-\infty}^{\infty} \sigma(\mathcal{A}) \left[\int_{S}^{\infty} \sigma(s) \right] d\mathcal{A}$$

Integrated forms of this reliability equation are available for normal, lognormal gamma, extreme value and other common statistical distributions. Refering to the normal distribution, the reliability estimate is essentially simplified to computation of the mean values and standard deviations of the stress and strength distributions. Then with the applied stress and strength probability density distribution,

$$\sigma(\mathcal{A}) = \frac{1}{S_{\mathcal{A}}\sqrt{2\pi}} \exp^{-\frac{1}{2}\left(\frac{\mathcal{A}-\bar{\mathcal{A}}}{S_{\mathcal{A}}}\right)^2}$$

$$\sigma(s) = \frac{1}{S_{s}\sqrt{2\pi}} \exp^{-\frac{1}{2}\left(\frac{S-\bar{S}}{S_{s}}\right)^2}$$

$$\bar{\mathcal{A}}, \bar{S} = \text{mean values}$$
$$S_{\mathcal{A}}, S_{s} = \text{standard deviations}$$

The reliability is simply calculated from

$$R = \frac{1}{\sigma_G \sqrt{2\pi}} \int_0^\infty \exp^{-\frac{1}{2}\left[\left(\frac{G-\bar{G}}{\delta_G}\right)^2\right]} dG$$

where
$$G = S - \lambda$$
$$\bar{G} = \bar{S} - \bar{\lambda}$$
$$\delta_G = \sqrt{\delta_\lambda^2 - \delta_S^2}$$

Kececioglu (11) has also described a transform method to evaluate the general reliability expression.

$$R = \int_{-\infty}^\infty \left[\int_\lambda^\infty \sigma(s)\,ds\right]\sigma(\lambda)\,d\lambda$$

Introducing the notation

$$G = \int_\lambda^\infty \sigma(s)\,ds$$

$$F = \int_\lambda^\infty \sigma(\lambda)\,d\lambda$$

Then
$$R = \int_0^1 G\,dF$$

where $dF = \sigma(\lambda)\,d\lambda$

and unreliability is expressed as

$$Q = \int_{-\infty}^\infty \left[\int_S^\infty \sigma(\lambda)\,d\lambda\right]\sigma(s)\,ds$$

by letting
$$G(S) = \int_S^\infty \sigma(s)\,ds$$

$$F(\lambda) = \int_S^\infty \sigma(\lambda)\,ds$$

Then
$$Q = \int_0^1 F\,dG$$

where
$$dG = \sigma(s)\,ds$$

60

Alternatively the reliability expression can be written

$$= \int_{-\infty}^{\infty} \left[\int_{-\infty}^{S} \sigma(\measuredangle) \, d\measuredangle \right] \sigma(s) \, ds$$

and letting

$$F(\measuredangle) = \int_{-\infty}^{S} \sigma(\measuredangle) \, ds$$

$$G(s) = \int_{-\infty}^{S} \sigma(s) \, ds$$

Then

$$R = \int_{0}^{1} F \, dG$$

where

$$dG = \sigma(s) \, ds$$

and

$$Q = \int_{-\infty}^{\infty} \left[\int_{-\infty}^{\measuredangle} \sigma(s) \, ds \right] \sigma(\measuredangle) \, d\measuredangle$$

where

$$G(s) = \int_{-\infty}^{\measuredangle} \sigma(s) \, ds$$

$$F(\measuredangle) = \int_{-\infty}^{\measuredangle} \sigma(\measuredangle) \, d\measuredangle$$

so that

$$Q = \int_{0}^{1} G \, dF$$

with

$$dF = \sigma(\measuredangle) \, d\measuredangle$$

61

Thus in applying this method, a principal decision concerns selection
of the appropriate statistical forms. This is obviously based on the
strength data and knowledge of the stress distribution. Note that the
technique does not incorporate volume dependency; nor variation of material
moduli, loadings, or structural geometry.

DETERMINATION OF STRESS DISTRIBUTIONS

MONTE CARLO TECHNIQUE

It is well known that stress is generally a function of many variables, i.e.

$$\sigma = \sigma(L, T, G, p, t, k)$$

where L through k represent loading, temperature, geometry, material properties,
time, stress concentration factors, etc. The Monte Carlo Technique is aimed
at determining the influence of these variables on the stress distribution
function.

A brief summary of the technique described by Kececioglu(12) is as follows:

1. Divide each distribution of the   variables into a number of intervals,

$$C_{ij} = \left(\frac{\sum N_j X_j}{\sum n_j}\right)_i$$

P_{ij} = area under curve for kth interval of the distribution of the ith variable.

62
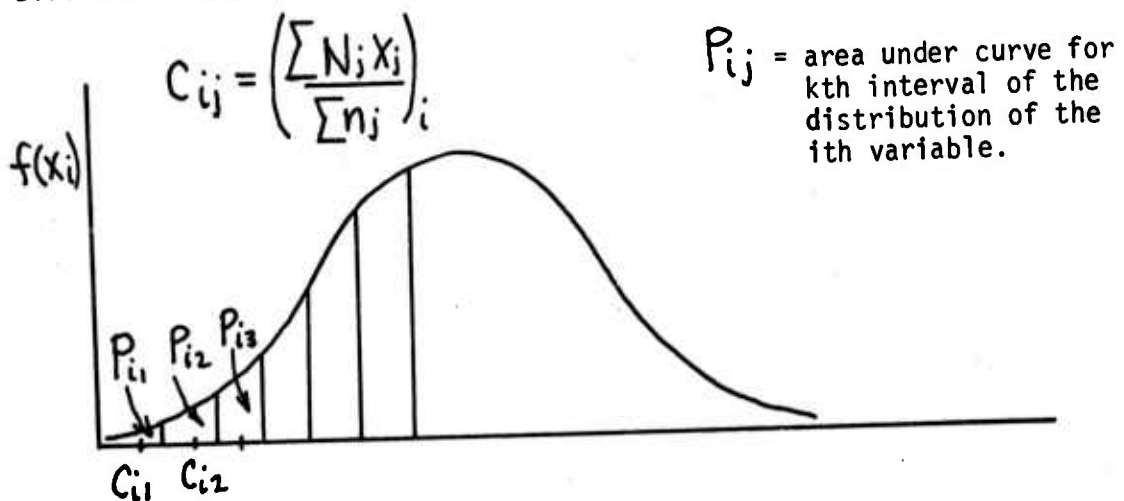
2. Calculate the centroids C_{ij}, $i = 1, 2, \cdots m$; $j = 1, 2, 3, \cdots, m$
for all the intervals in each distribution.

3. Determine the probability of occurance of the centroid of each
interval, P_{ij} , which is the percentage of the ith distribution curve
contained in the jth interval

4. Enter all the pairs of numbers, C_{ij} , and P_{ij} , into a digital
computer, along with a random number generating program and a program
for associating particular digits in the random njmbers with a particular
pair of C_{ij} and P_{ij} values of that variable.

5. Generate a random number and identify a complete set of C_{ij} values
for all variables associated with it, together with their associated
probabilities P_{ij}

6. Calculate the stress value from each set of the randomly selected
variables.

7. For each value of stress, determine the product of the interval
probabilities associated with the C_{ij} values used.

8. Determine a suitable number of intervals for the calculated stress
values and group these stresses and probabilities into suitable intervals.

9. Calculate the centroid stresses for each interval; these are abscissas
of the $\sigma(\Delta)$ distribution.

10. Determine the probability of occurance associated with the centroid
stresses by summing up the probabilities in the interval. These are the
ordinates.

11. These resulting distributions now are fitted by statistical regression
analysis (normal, log normal, Weibull)and the distribution with the highest
correlation factor is chosen.

The discussion so far has used a maximum principal strength No consideration has been made of the appropriate failure theories for combined stresses. However, regardless of the failure theory applied, the formal logic outline here is relevant.

It is apparent that a number of formal statistical treatments can be applied to estimate the reliability of a subcomponent. Choice of the appropriate method is intimately related to results obtained under simulated service conditions. Data currently being obtained on the ARPA-FORD-WESTINGHOUSE Ceramic Turbine project will provide the information to discriminate between these treatments.

4.0 FRACTURE MECHANICS CONSIDERATIONS

Fatigue & Fracture

Fracture mechanics approaches emphasize visible, geometrically defined crack and the resistance of a given material to its slow or sudden growth under load. Sudden crack growth phenomena is based on a well defined theory, particularly for brittle materials, whereas slow growth relies rather heavily on procedures of experimental materials evaluation. Which is to say that the theoretical approach based on the instability condition uniquely defines the start of fast propagation whereas slow crack growth dependence on stress intensity range is often a purely empirical correlation, and subject to significant statistical variation. Nonetheless fracture mechanics procedures have provided an engineering approach to deal with cracked or flawed structure and allow generally conservative estimates to be made of service life.

The usual application of linear elastic fracture mechanics involves two major steps. First of all a conventional stress analysis is conducted of the structure under consideration, ignoring the presence of defects. Usually this detailed stress information is then coupled with simplified stress intensity calculations using mathematical models which resemble the actual situation with respect to geometric boundaries, stress distribution and defect characteristics. Successful utilization of fracture mechanics theories is also dependent on adequate information concerning materials properties, existing defects, as well as knowledge of stress conditions. The following materials properties are ordinarily necessary for various fracture mechanics considerations:

K_{IC} or G_{IC} - plane strain fracture toughness

       σ_Y - conventional tensile yield strength

       E - Young's modulus

       ν - Poisson's ratio

      $\dfrac{\partial a}{\partial N}$ - crack growth rate (increase in crack length per fatigue cycle) as a function of the stress intensity and stress history

The basic toughness parameter K_{IC} is essential in all considerations, from a simple comparison of materials to a complex calculation of allowable defect sizes.

It should be recognized that K_{ic} is influenced by many factors. For instance K_{IC} can be measured via a variety of test methods and this can introduce additional scatter in the observations. Hence it is essential that the designer be certain that the test material condition, notch orientation and test procedures used for fracture toughness measurements be fully representative of the component of interest.

A number of examples are available in the literature to estimate the importance of numerous variability factors for metals and ceramics. These include the recent evaluation of fracture mechanics data for the F-111 aircraft (13). Swanson and Gross (14) for example, have reported variation in the order of 8% for K_{IC} values for alumina oxide, whereas variation of twice this magnitude are not uncommon for certain ceramics.

Fracture toughness of materials is measured by a variety of test methods. Three of the common types of experiments include the compact

tension (CT) surface flaw (SF) and double cantilever beam (DCB) types of specimens. Figure 15 illustrates these configurations.

Room temperature crack growth tests were performed at AMMRC on hot pressed and reaction sintered silicon nitride using a form of compact tension specimen. Only initial fracture loads could be measured as the crack rapidly propagated across the specimen. The contoured double cantilever form was also tried at room temperature with similar results. Both configurations will be used at elevated temperature to determine whether the technique is suitable.

Thus far slow crack growth data has been reported by Evans & Wiederhorn (15). They employed an edge notched plate, under condition of edge twist and for constant displacement rate conditions. The specimen is shown schematically in Figure 16.

DISC TESTING FOR FRACTURE TOUGHNESS DETERMINATION

We have seen that fracture toughness of materials, considered as an inherent property, can be experimentally determined by a variety of methods such as notched tension specimens, notched flexure beams, edge notched plates. Bursting of a notched or otherwise pre-flawed disc can also be used to measure crack behavior under biaxial stress conditions. Actual determination of this fracture toughness is valid provided that brittle fracture occurs and also provided that an accurate analysis exists for the experimental method.

In their early paper, Winne and Wundt (16) assumed that the Bowie solution (17, 18) for an infinite plate containing a notched hole, and the stress field in a rotating, bored and notched disc would have equivalent
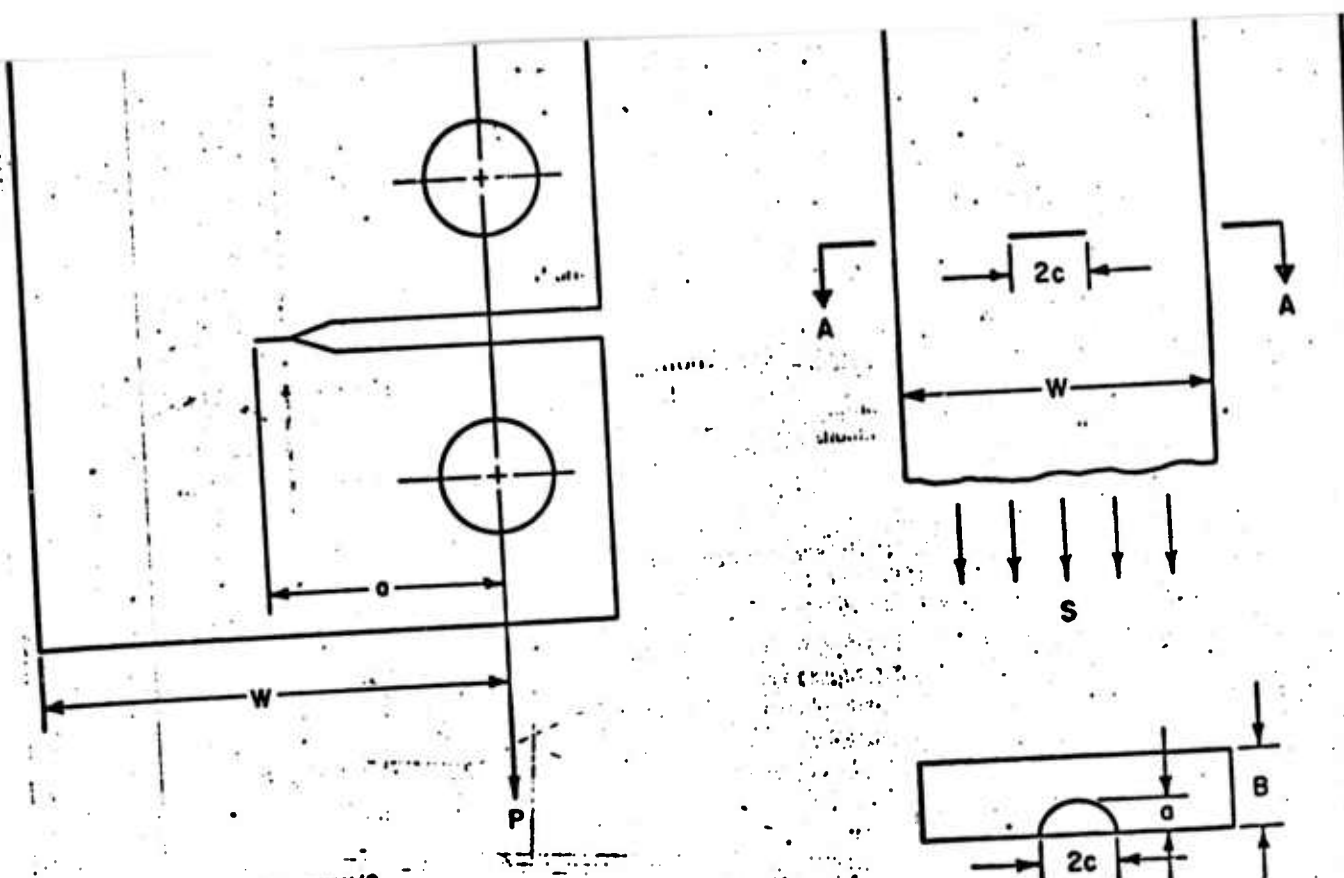
Nominal crack length, $a = W/2$

Nominal max. net section stress $= S_{net} = \dfrac{4P}{B(W-a)^2}(W + a/2)$

Section A-A

CONFIGURATION AND GEOMETRY OF COMPACT TENSION SPECIMEN

CONFIGURATION AND GEOMETRY OF FLAW SPECIMEN
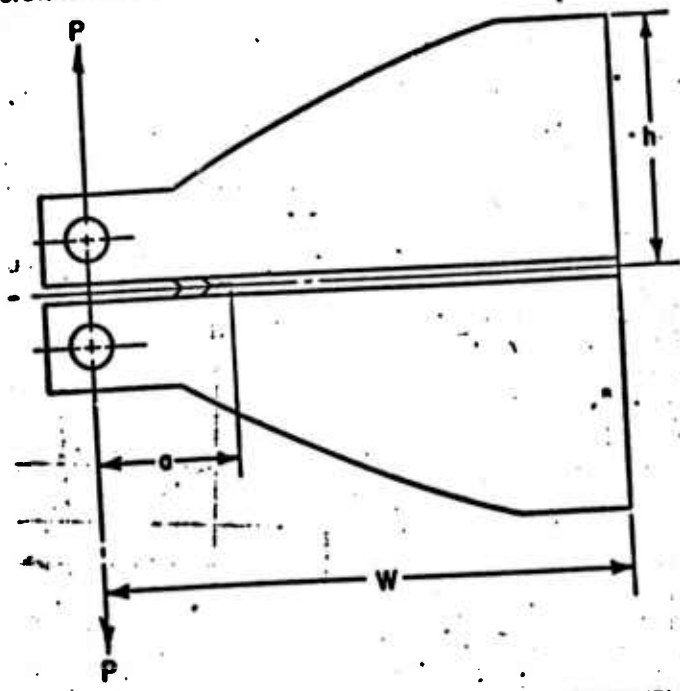
CONFIGURATION AND GEOMETRY FOR TAPERED DOUBLE-CANTILEVER BEAM
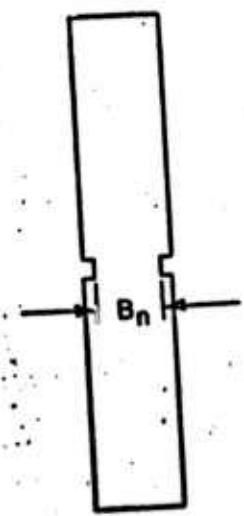
Figure 15. Typical Crack Growth Specimens, Compact Tension, Double Cantilever Beam and Surface Flaw.

68
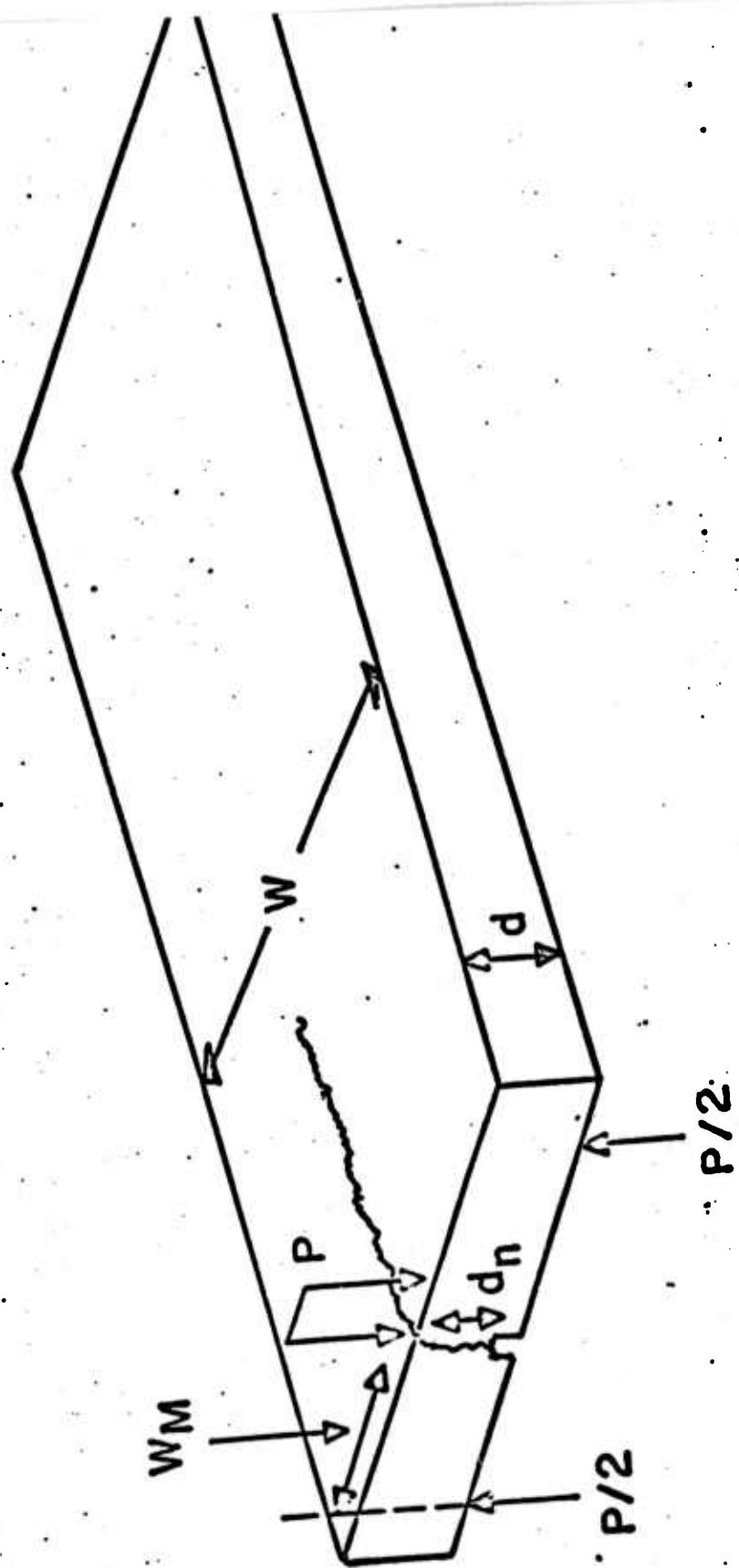
Figure 16. Edge Twist Plate Specimen for Crack Growth Studies.

69

stress distribution around the holes and cracks, provided the overall crack length, L satisfied the condition

$$D_1 + 2L < \frac{1}{4} D_2$$

where D_1 - diameter of disc bore and D_2 = outer diameter of disc. This criteria was chosen by analogy to the case of an infinite flawed plate as contrasted to a finite width center flawed plate. Analytical results for the finite sized disc have been completed by Freese and this permits examination of the validity of the stated criteria, as well as reassessment of the use of discs to measure fracture toughness. The results of the stress intensity computation are shown in Figure 17. Using the same formal procedure outlined by Winne & Wundt, a notch geometry can be chosen to induce brittle fracture and the corresponding value of K_{IC} can be determined.

The analytical results indicate the marked effects of geometry on the stress intensity, and it is obvious that the fracture behavior of the disc is dependent on notch geometry. Thus it is not possible to evaluate or compare materials characteristics on the basis of failure behavior of notched discs of arbitrary geometry.

In order to observe fracture toughness of the material, it is necessary to cause failure via brittle, crack induced fracture at stresses considerably below the tensile strength of the specimen. Given the fracture toughness of the material and the solution for stress intensity, we can equate this to maximum stresses induced in a thin rotating disc.

The procedure would allow comparison of fracture toughness results under loading rates, biaxiality and temperatures similar to the turbine engine environment.

a			
.1	.6541	.6375	.6356
.2	.8571	.8284	.8279
.4	1.1046	1.0509	1.0393
.6	1.2853	1.1974	1.1796
.8	1.4447	1.3167	1.2910
1.0	1.5975	1.4221	1.3892
1.2	1.7503	1.5197	1.4743
1.4	1.9071	1.6127	1.5552
1.6	2.0707	1.7030	1.6318
1.8	2.2933	1.7919	1.7033
2.0	2.4268	1.8802	1.7766
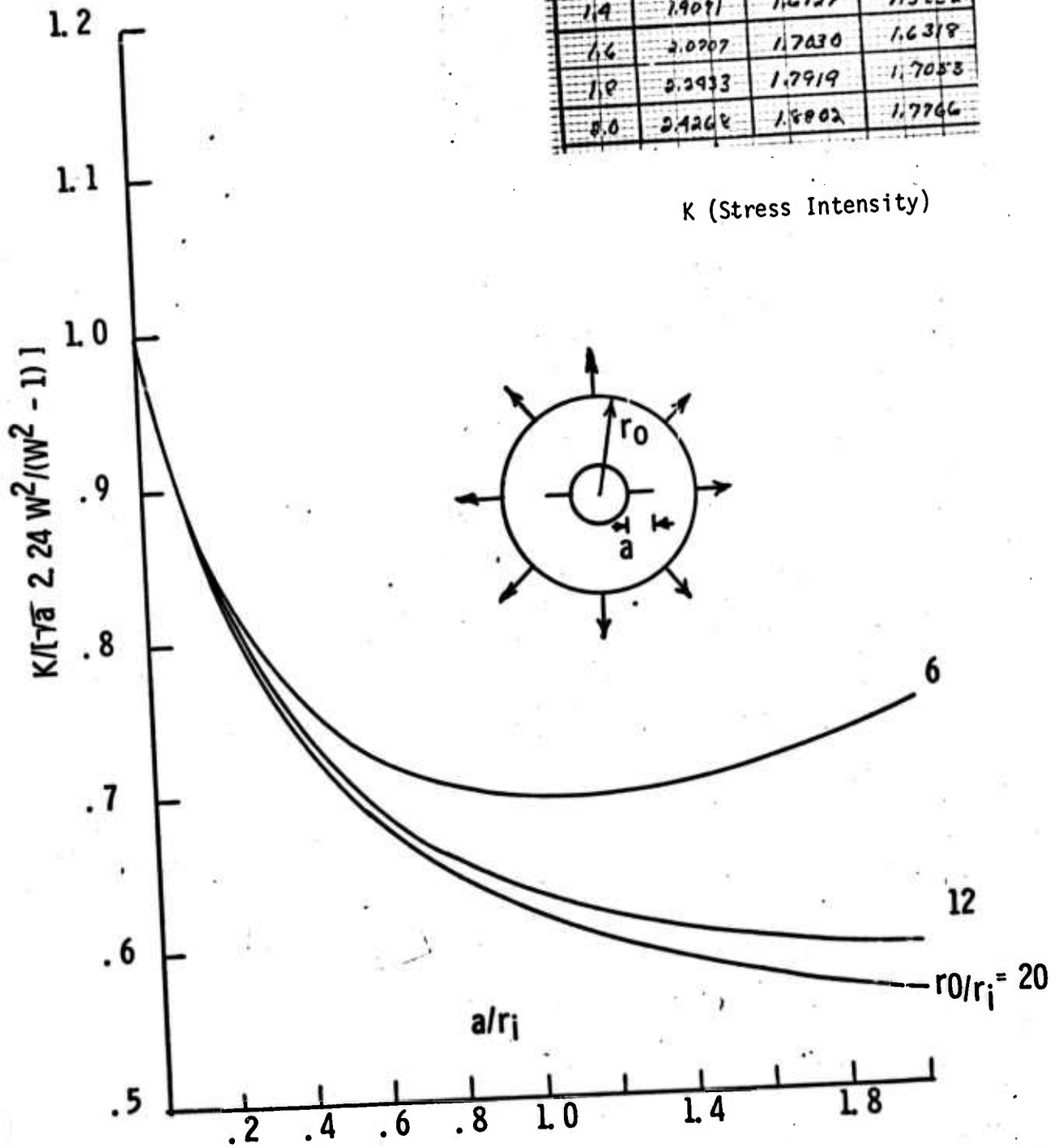
K (Stress Intensity)

Figure 17. Stress Intensities For Notched Disc.

71

Flaw Size Reduction

There is obviously potential substantial benefit associated with studies of fracture initiating flaws in the materials. It is reasonable to assume that low strengths will be enhanced by some factor proportional to the square root of the flaw size. Furthermore, if the source of the fracture initiating flaws can be determined, then appropriate fabrication controls can be instituted to effect the desired strength enhancement. In order to apply fracture mechanics considerations, it must be established that the crack extension conditions for flaws that control strength are similar to gross, geometrically defined cracks on which stress intensity computations are based. Barring this possibility, the next obvious requirement is to at least investigate how well elementary fracture mechanics predictions apply to these particualr ceramics.

These computations must be based on detailed fractography of the specimens.

4.1 FRACTOGRAPHY

Fractographic analysis can be used for a variety of purposes. Two common applications are a) to determine the location and size of fracture origin in order to provide data for fracture mechanics analysis, and b) to elucidate the nature of the defects causing a fracture to initiate, relate this flaw to the material process, then use this information to improve the production method such that critical flaws are eliminated, diminished in size or frequency of occurance.

During this program, fractographic analysis was completed in both of these areas. As mechanical test specimens having clearly defined fracture origins become available, they will be examined in the Scanning Electron microscope (SEM) with respect to geometry, microstructure (and microtopography) as well as for chemical compositions of various regions or phases of interest using the non-dispersive X-ray (NDX) unit which is attached to the SEM.

Of the fractures examined to date, fractures have originated both internally and on the surface of the specimens. When fractures initiate within the central portion of the bars, the initiating flaw is the intrinsic strength limiting flaw, and not a possible machining artifact. Thus the hot pressed silicon nitride (HPSN) specimens with interior fracture origins were subjected to special scrutiny.

GEOMETRIC CONSIDERATIONS

The HPSN tension and flexure specimens described in Tables   and   were carefully examined and typical flaw geometries were documented. A typical tensile fracture face for interior failure origin appears in Figure 18.

73

1740X Magnification

17X Mag

870X

175X
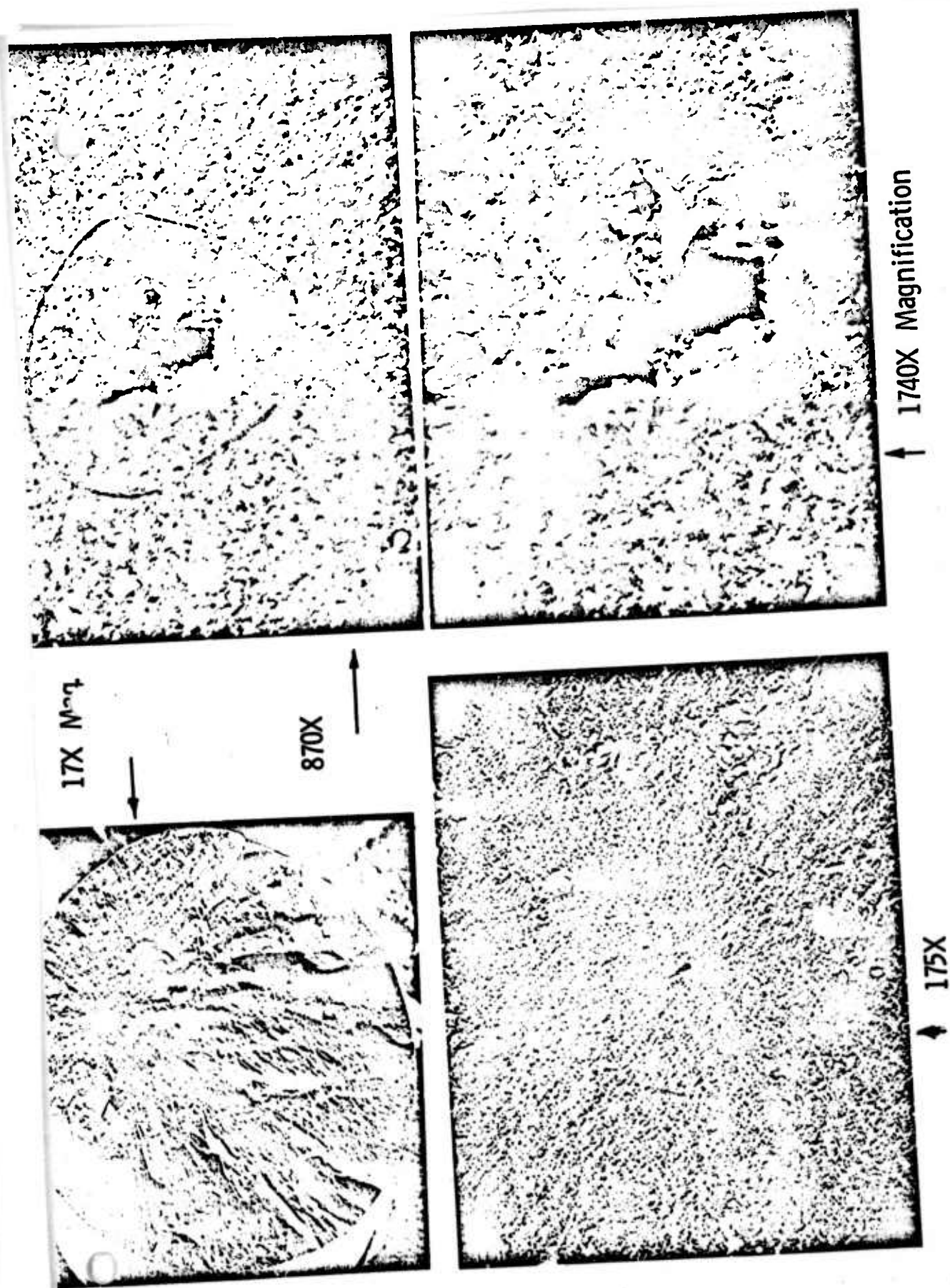
Figure 18 Fracture Origin in Specimen Number 10

74

while schematics of the flaw geometries observed to date are shown in Figures 19, 20, 21. Similar results for the flexure specimens are shown in Figure 22. In idealizing these flaws, the gross shape was determined at fairly low magnifications since observation of the details using the scanning electron microscope tended to obscure the shape of the flaw.

COMPOSITION AND SOURCE OF FLAWS

Examination of the fracture surfaces of available specimens indicates that there are flaws, inclusions or second phase particles larger than the initiating flaw. Therefore a key problem to be addressed in the fractographic portion of this program is identification of the nature of the fracture initiating flaws and how these differ from the non-fracture initiating material defects. Resolution of this matter will undoubtedly provide insight into procedures to improve strength and the distribution of strength.

All flaws have been examined and characterized chemically by non-dispersive X-ray techniques (NDX) and the composition of the flaw is compared to the average material composition. In practice the NDX unit on our scanning electron microsocope is sensitive to elements with atomic numbers higher than Mg's. Therefore N_2, O_2 or Mg is not detected in our routine studies. The equipment should detect Mg, but it is in fact lost in nosie at the end of the scale. Note that the vertical axis of the NDX traces in Figures 23 and 25 have been considerably expanded, resulting in a noisy pattern. The instrument actually reads out electronically the Kev associated with a given peak. Thus the ambiguity suggested in these figures is not in fact present.
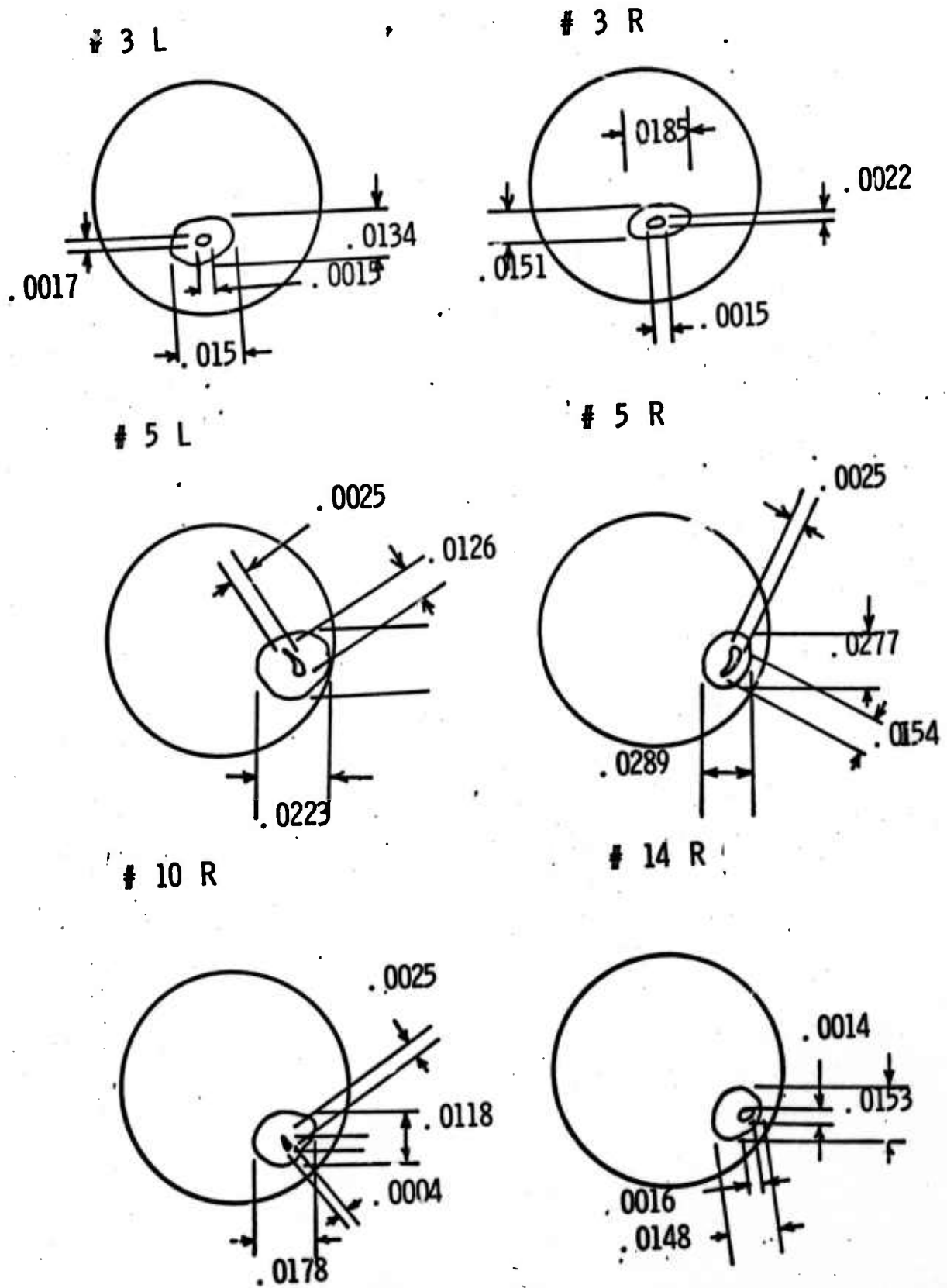
Typical Defects in Tension Specimen, No. 3, 5, 10 and 14

Figure 19.
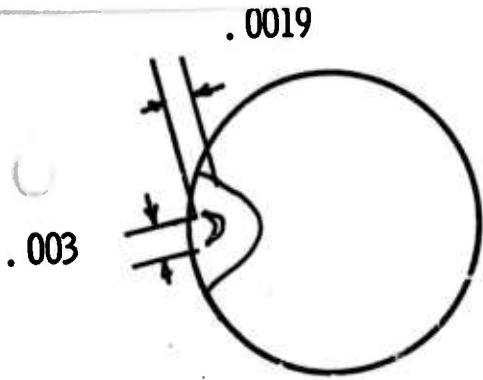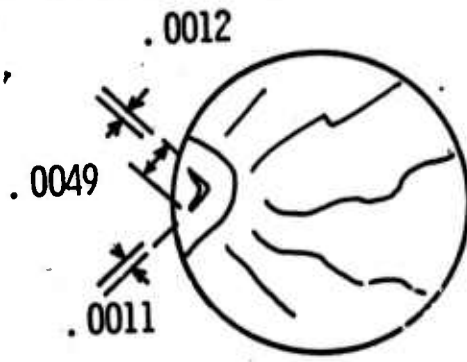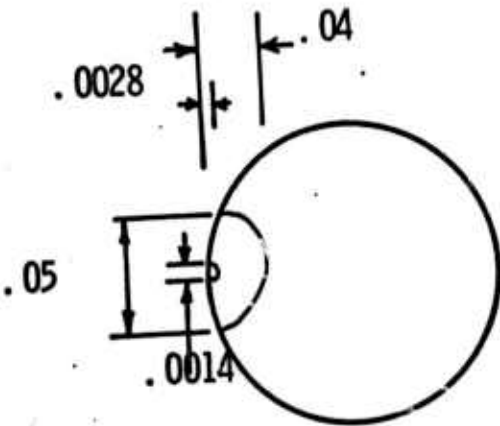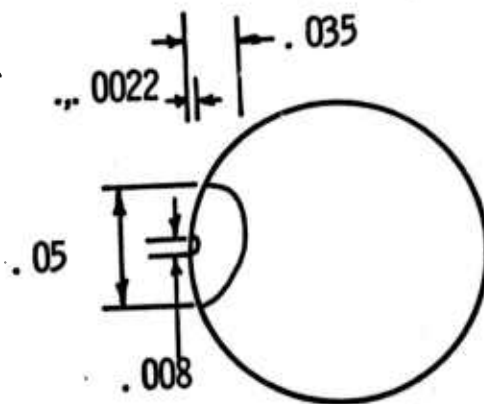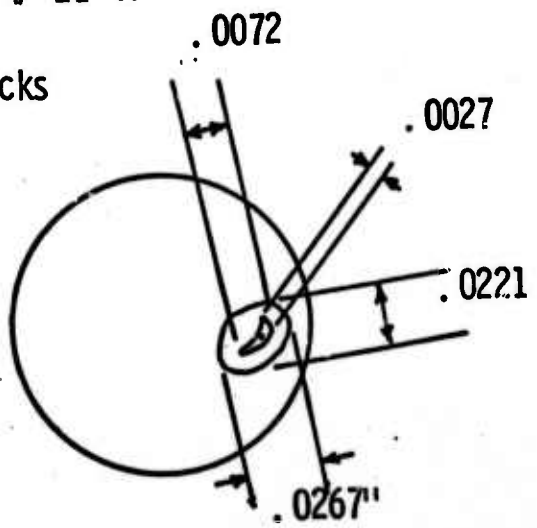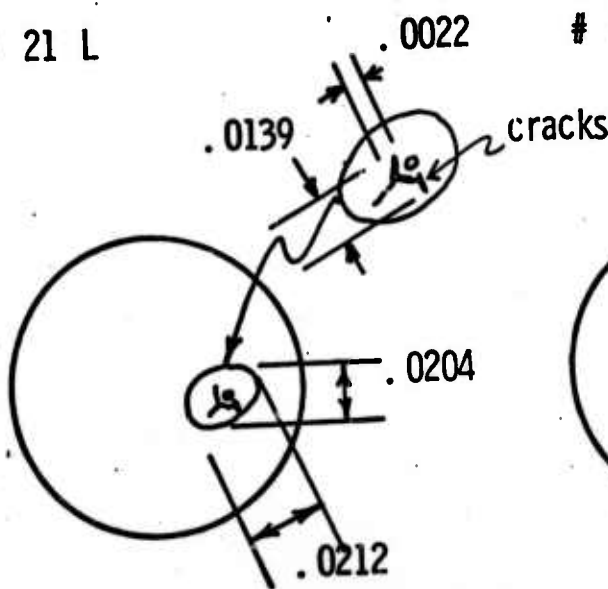
Typical Defects in Tension Specimen, No. 16, 20 and 21

Figure 20.

Specimen Number   Typical Defect Sizes

17 L
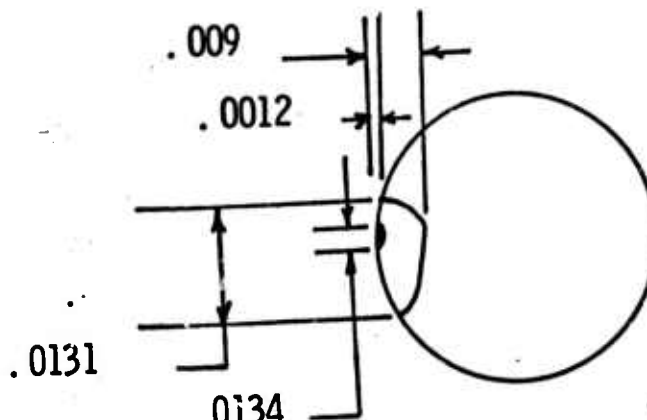

```
      .009
     .0012

.0131
  .0134
```
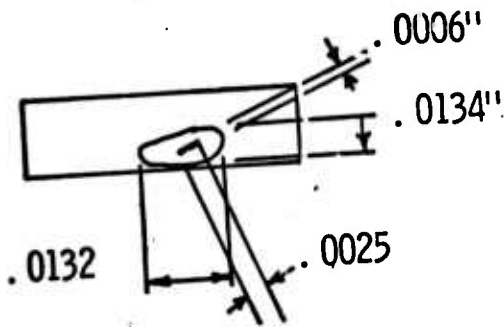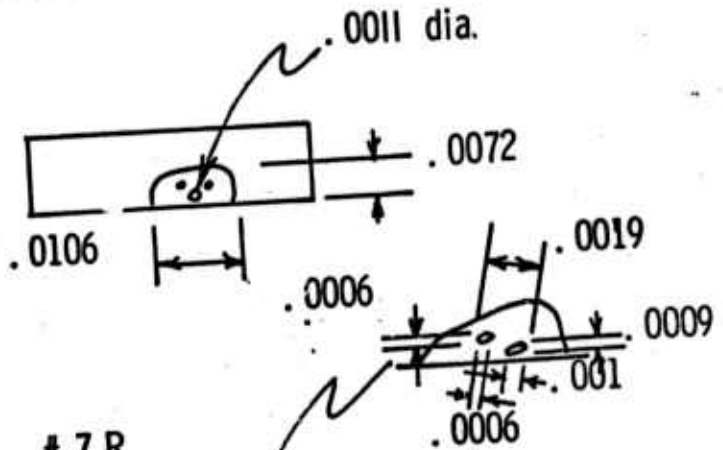Other Observed Defect Sizes

Specimen

4 R   .0007, .0009, .0010, .0012

4 L   .0005, .0007 .0009, .0013

11 R   .0024,   .0013 .0019, .0016,   .0010

12 L   .0009,   .001 .0011,   .0014

12 R   .0005, .0006, .0007, .0011, .0012

#16 L   .0009, .0011,   .0013 ,.0013

16 R   .0011, .0013, .0015,   .0017

20 R   .0007, .0011, .0016, .0018, .0019

20 L   .0006, .0007,   .0008, .0010

Typical Defects in Tension Specimen, No. 4, 11, 12, 16 and 20

Figure 21.   78

Specimen # 7 L

10 R

.0006"

.0134"

.0132   .0025

.0011 dia.

.0072

.0106

.0006

.0019

.0009

.001

.0006

#10 L

.008

.0109   .001 dia.

7 R

.0075

.0105

14 L

.018

516   .0094

.0017

16 R

.0027

.0112"

.0027

.0153
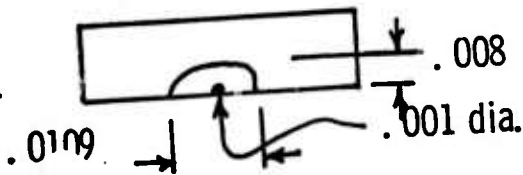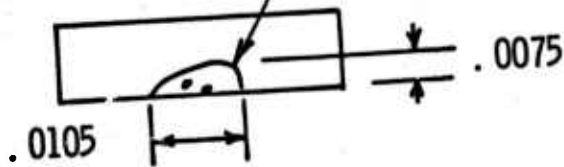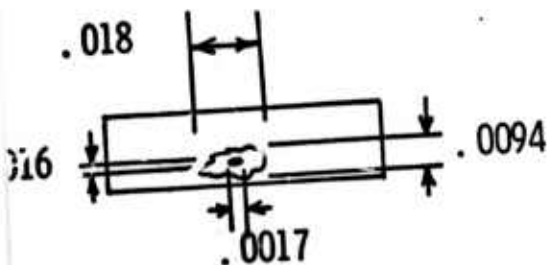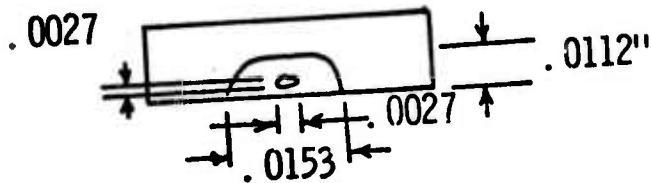
Schematic of Flexure Specimen Flaw Origins

Figure 22

79

A detailed examination of four interior fracture origins indicates that:

a) Fractures initiate in regions of incomplete densification with large amounts of interconnected porosity (See Figure 23 and a and b).

b) Inclusions or second phases do not apparently initiate fracture.

Such areas of high porosity have been observed to be the initiation sites for fracture in other ceramics. In the hot pressed silicon nitride examined here, there is a tendency for elements such as Ca, V, Mn, Co, Ba and in some instances Fe to preferentially segregate to the areas in which the fracture originates. In second phase particles which were not fracture initiation sites, Al, Mo, Ca, and Fe have been observed preferentially. However, based on the limited available data so far it is premature to attribute the high porosity-low density regions of fracture origin to any specific impurity or combination of impurities.

b) Portion of critical flaw, 900x

a) General area showing fracture mirror
v, indicates orilgion 35x
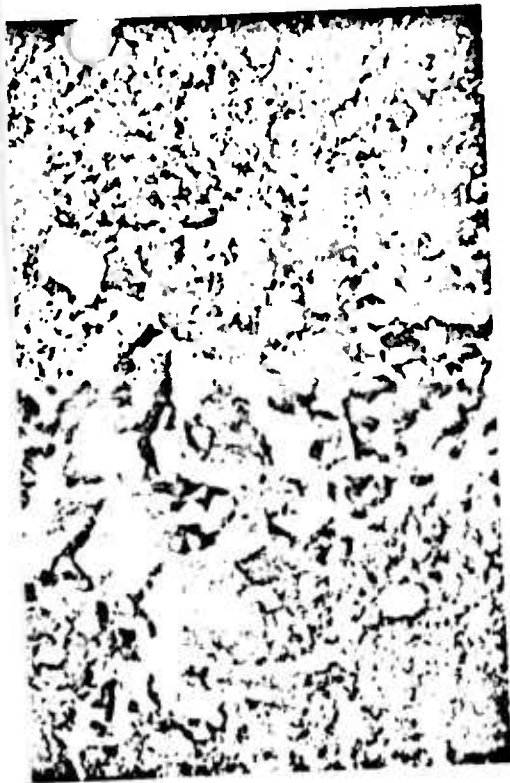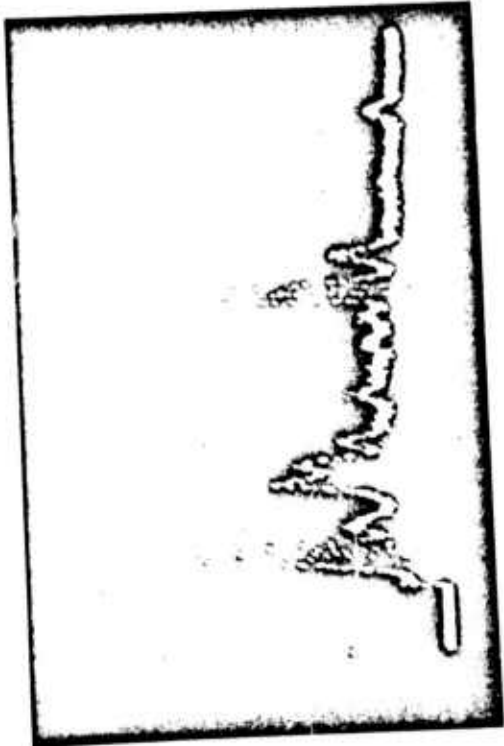
d) NDX - Analysis of area shown in c)
in SAMPLE #2l

c) Nature of incomplete bond shown at 4500x
FRACTURE

Photomicrographs and NDX Analysis, Tension Specimen No. 21
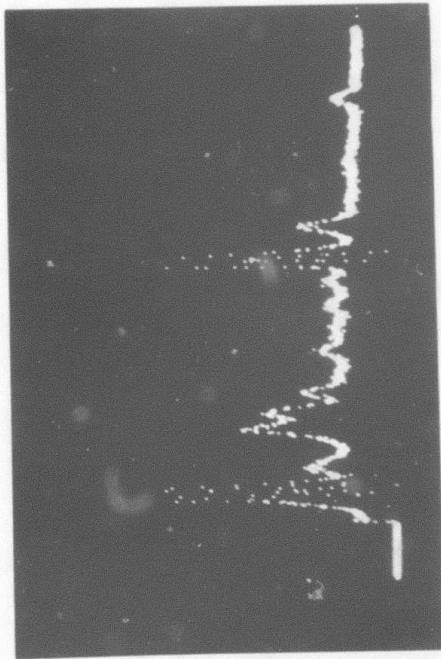
Figure 23.   81

a) General area showing fracture mirror
   v, indicates orijion   35x
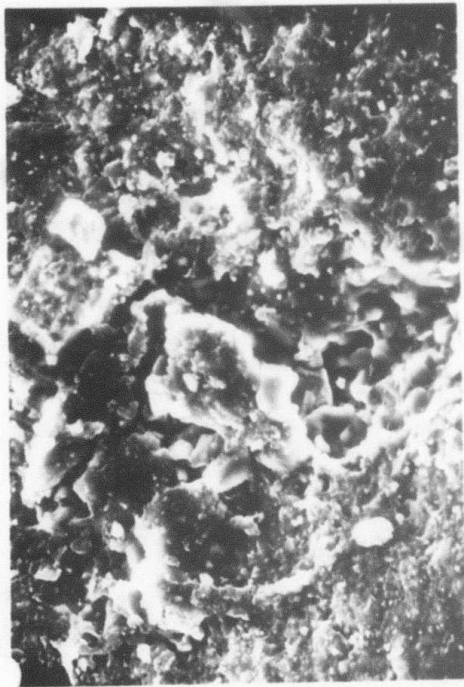
b) Portion of critical flaw , 900x
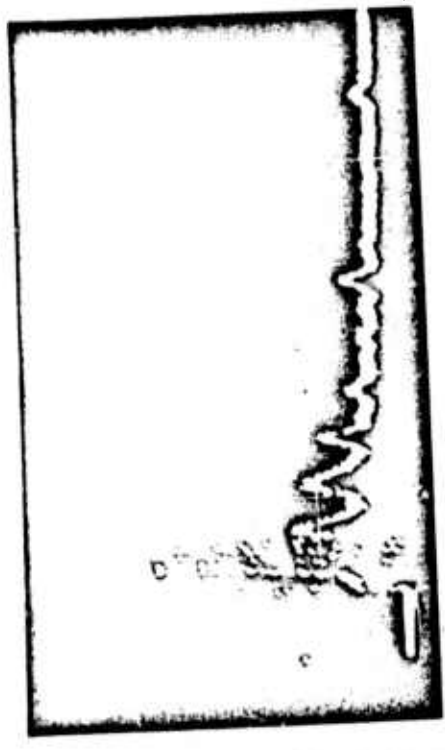
c) Nature of incomplete bond shown at 4500x
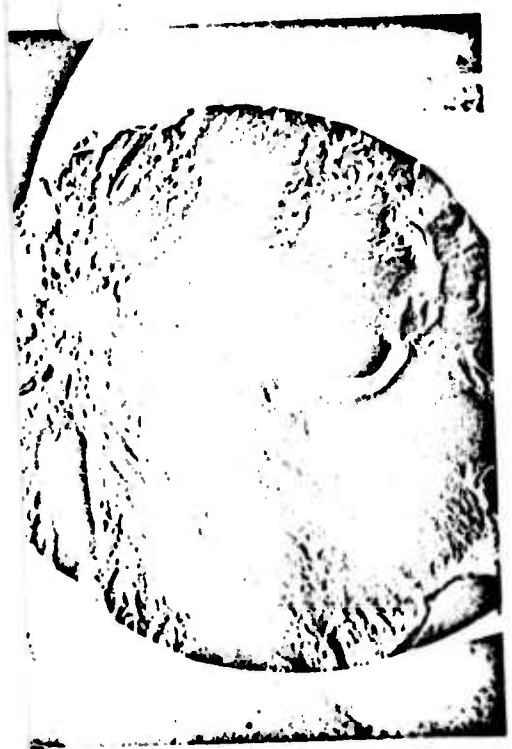
d) NDX - Analysis of area shown in c)

FRACTURE ORIGIN IN   SAMPLE #21
ARMY MATERIALS AND MECHANICS RESEARCH CENTER

19-066-900/AMC-73

b) Fracture mirror & origion
origion indicated by, V, 45x

d) NDX -Analysis of area in center
of c)

in SAMPLE # 10

a) View of entire fracture, 18x

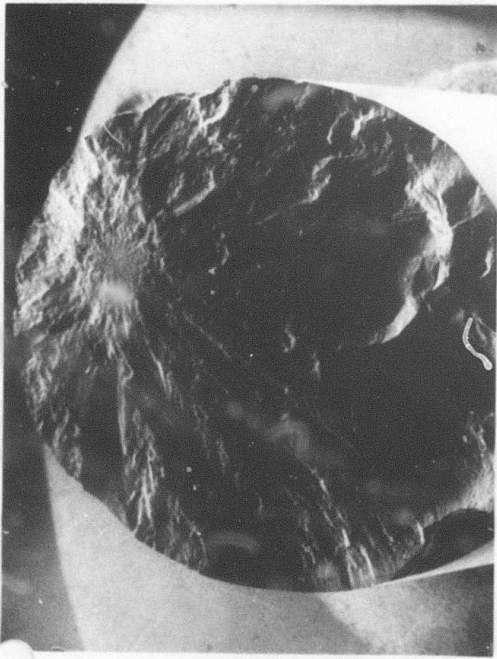c) Part of area of interconnected porosity
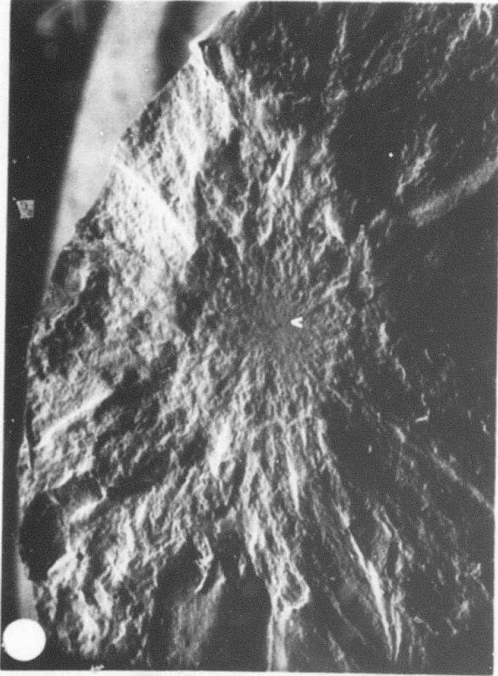at origion of fracture 1800x

FRACTURE

Photomicrographs and NDX Analysis, Tension Specimen No. 10
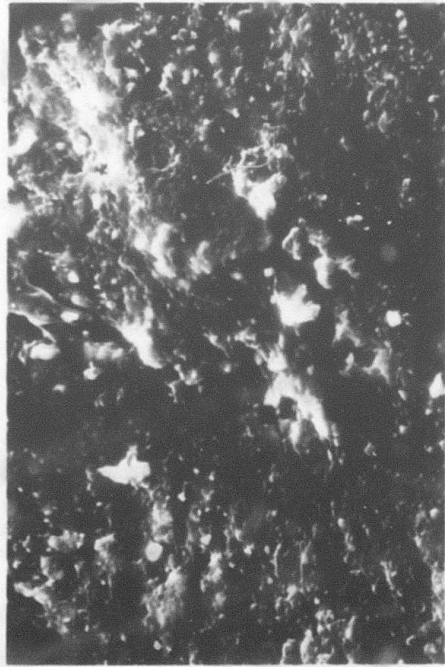
Figure 24.

82

a) View of entire fracture, 18x

b) Fracture mirror & origion
origion indicated by, v , 45x

c) Part of area of interconnected porosity
at origion of fracture 1800x

d) NDX -Analysis of area in center
of c)

FRACTURE

SAMPLE # 10

ARMY MATERIALS AND MECHANICS RESEARCH CENTER

19-066-899/AMC-73

REFERENCES

1. a) McLean, A.F., Fisher, E.A. and Harrison, D.E., "Brittle Materials Design, High Temperature Gas Turbine", AMMRC CTR 72-3, Interim Report, July 1, 1971 to December 31, 1971.

   b) McLean, A.F., Fisher, E.A. and Bratton, R.J., "Brittle Materials Design, High Temperature Gas Turbine", AMMRC CTR 72-19 Interim Report, January 1, 1972 to June 30, 1972

   c) McLean, A.F., Fisher, E.A. and Harrison, D.E., "Brittle Materials Design, High Temperature Gas Turbine", AMMRC CTR 73-9

   d) McLean, A.F., Fisher, E.A. and Harrison, D.E., "Brittle Materials
   - Design, High Temperature Gas Turbine", AMMRC CTR 73, Report in Press.

2. Baratta, F.I. and Driscool, G.W., "A New Axial Tension Testor for Brittle Materials, January 1969.

3. Weibull, Waloddi, "A Statistical Theory of the Strength of Materials, Ingeniors Vetenskaps Akadamien-Handlingar, Stockholm, No. 151, pp. 1-45, 1939.

4. Weibull, Waloddi, " The Phenomena of Rupture in Solids, Ingeniors Vetenskaps Adadamien-Handlingar, Stockholm, No. 153, pp. 1-55, 1939.

5. DeSalvo, G.J. and Stanchik, R.M., "Theory and Structural Design Applications of Weibull Statistics, Westinghouse Astronuclear Laboratory, WANL-TME-2688, May 1970.

6. Robinson, E.Y., "Some Theoretical and Experimental Aspects of Design With Brittle Material", University of California Report, UCRL-7729, August 1964.

7. Daniel, I.M. and Weil, N.A., "Influence of Stress Gradient Upon Fracture of Brittle Material ASMR Paper 63.

8. Bolotin, V.V., "Statistical Methods in Structural Mechanics", Holden Day Inc., 1969

9. Haugen, E.B., "Probabilistic Approaches to Design", John Wiley and Sons, 1968

10. Epstein, B., "Statistical Aspects of Fracture Probelsm", Journal of Applied Physics, Vol. 19, 1948

11. Kececioglu, D. and Cormier, D., "Designing a Specified Reliability Directly into a Component", Proc. Third Annual Aerospace Reliability and Maintainability Conference, July 1964, pp. 546-565

12. Kececioglu, D., "Reliability Analysis of Mechanical Components and Systems", First International Conference on Structural Mechanics in Reactor Technology Paper M 1/4, Berlin 20-24, September 1971.

13. Feddersen, C.E., Moon, D.P., Hyler, W.S., "Crack Behavior in D6AC Steel, An Evaluation of Fracture Mechanics Data for the F-111 Aircraft, MCIC-72-04, January 1972.

14. Swanson, G.D. and Gross, G.E., "Factor Analysis of Fracture-Toughness Test Parameters for Al_2O_3, Journ. Amer. Ceramics Soc., Vol. 54, No. 8, August 1971.

15. Evans, A.G. and Wiederhorn, S.M. "Crack Propagation and Failure Prediction in Silicon Nitride at Elevated Temperatures".

16. Winne, D.H. and Wundt, B.M., "Application of the Griffith-Irwin Theory of Crack Propagation to the Bursting Behavior of Discs, Including Analytical and Experimental Studies", Transactions ASME, October 1957.

17. Bowie, O.L., Analysis of an Infinite Plate containing Radial Cracks Originating at the Boundary of an Internal Circular Hole, Journal of Mathematics and Physics, Vol. 25, April 1956, pp. 60-71.

18. Bowie, O.L., Effect of Crack Length on the Rupture Stress for Brittle Failure of Hollow Cylinders Contining Radial Cracks at the Bore, Watertown Arsenal Laboratory Report, WAL 893/167, Aug 5, 1954.